Charles University in Prague

Faculty of Mathematics and Physics

DOCTORAL THESIS

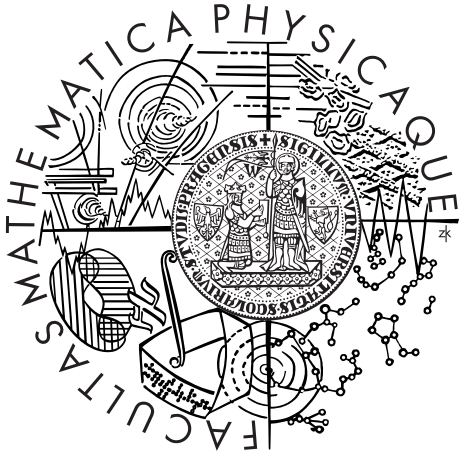

Jaroslav Kočišek

Implementation of ion imaging technique in experiments with free molecules, clusters and nanoparticles

Department of Surface and Plasma Science

Supervisor of the doctoral thesis: Michal Fárník

Study programme: Physics

Specialization: Physics of Plasma and Ionized Media

Prague 2013

Acknowledgment

The thesis would not have been finished without contributions, which I would like to acknowledge here.

At first, I have to thank people responsible for the first step to present thesis - my move to Prague. The first one is my friend Juraj Fedor who seeds a crazy idea of second doctorate into my mind. The second one is my supervisor Michal Farnik who made significant efforts to employ me for the Marie Curie position. Both are easygoing persons and brilliant scientists and so I had an excellent opportunity to improve my knowledge and scientific skills, which I fully utilize. I appreciate Michal's superb managerial skills, which allows me to work on leading edge scientific projects and use state of the art equipment. He always knows how to direct my efforts the most productive way.

My thanks go to my inTeMate (in Tennis Mate) Jozef Lengyel for the most successful measurements we did on CluB experimental setup. I would like to thank people who explains me the CluB experiment Andryi Pysanenko and Viktoria Poterya for perfect bowling plays. I am grateful to Ondrej Votava and Petr Slavicek for amazing amount of new information I get from our scientific discussions, which range from Fohn winds to Vysehrad Cemetery. I thank Pavla Svrckova and Pavel Kostal for keeping my brain fit by continuous support of excellent cookies. And I have to thank all together for great time I spent in the Molecular and Cluster Dynamics Group.

I have to thank Jana Safrankova who tolerates my ignorant behavior to my almost mater and people from Juraj Glosik group who try to cover it.

To the end, like always, I left the most important persons. I have to thank Monika and Nela for their unbelievable patience in waiting each day for daddy's coming home.

I declare that I carried out this doctoral thesis independently, and only with the cited sources, literature and other professional sources.

I understand that my work relates to the rights and obligations under the Act No. 121/2000 Coll., the Copyright Act, as amended, in particular the fact that the Charles University in Prague has the right to conclude a license agreement on the use of this work as a school work pursuant to Section 60 paragraph 1 of the Copyright Act.

In ..... date ..... signature of the author

Název práce: Implementace techniky iontového zobrazování ve fotodisociačním experimentu s volnými molekulami, klastry a nano částicemi ve vakuu

Autor: Jaroslav Kočišek

Katedra: Katedra fyziky povrchů a plazmatu

Vedoucí disertační práce: Mgr. Michal Fárník, PhD., DSc., Ústav fyzikální chemie J. Heyrovského, AV ČR, v.v.i.

Abstrakt: Experimentálna práca sa zaoberá implementáciou nových techník do oblasti štúdia klastrov a nanočastíc v molekulových zväzkoch. V rámci práce bol otestovaný systém kombinujúci pulzný molekulový zdroj klastrov s technikou iónového zobrazovania v konfigurácii mapovania rýchlostí. Následne bola rovnaká metóda implementovaná spolu s novým hmotnostným spektrometrom na zariadenie s molekulovým zväzkom veľkostne selektovaných klastrov. Nové metódy boli použité na štúdium vplyvu prostredia na foto a elektrónmi indukované reakcie klastrov. Medzi najdôležitejšie výsledky patrí ukázanie vplyvu expanzných podmienok na štruktúru formovaných klastrov HBr a C_2H_2. Výsledky experimentov s molekulami HNO_3 a CF_2Cl_2 sú potom dôležité pre pochopenie heterogénnych procesov v stratosfére.

Klíčová slova: iontové zobrazování, hmotnostní spektrometrie, molekulové svazky, fotchemie, nanočástice

Title: Implementation of ion imaging technique in experiments with free molecules, clusters and nanoparticles

Author: Jaroslav Kočišek

Department: Department of Surface and Plasma Science

Supervisor: Mgr. Michal Fárník, PhD., DSc., Ústav fyzikální chemie J. Heyrovského, AV ČR, v.v.i.

Abstract: The experimental work is focused on implementation of novel techniques to study clusters and nanoparticles in molecular beams. A new experimental system was tested, which combines the technique of velocity map ion imaging with pulsed molecular beam source. The same method and new mass spectrometer were implemented on the apparatus with molecular beam of size selected clusters. The new methods were used to study environmental effects on photo and electron induced chemistry. The most important results concerns on influence of expansion conditions on the structure of formed neutral clusters of HBr and C_2H_2. Results of experiments with HNO_3 and CF_2Cl_2 molecules are then crucial for understanding heterogeneous processes in the Stratosphere.

Keywords: ion imaging, mass spectrometry, molecular beams, photochemistry, nanoparticles

Contents

Preface

The thesis summarizes the research I conducted during my studies in the group of Michal Fárník at J. Heyrovský institute of physical chemistry in Prague. The main focus was on an implementation of the ion imaging technique to study photodisociation dynamics in a cluster environment. The ion imaging is already well established experimental approach to a photodissociation dynamics which allows to obtain the full vector information about a motion of photodissociation fragments. Technique is successively used in photoelectron spectroscopy of cluster anions. Photofragment ion dynamics of molecules deposited on the surface of large rare gas clusters were already studied too. In present work we focus on implementation of the technique to study dissociation dynamics of molecules inside clusters, and dynamics of large clusters, therefore exploring the solvent effect on the particular system.

A typical question rising up when reading a thesis, which presents experimental work of scientific group is about the particular contribution of the author. Therefore, I would like to spend few rows explaining my "Marie Curie" years with M. Fárník's Molecular and Cluster Dynamics group. First year I joined postdoctoral fellow Juraj Fedor, who was developing the test apparatus, which combines pulsed molecular beam source and photofragment ion imaging. Juraj introduced me to the technique and operation of lasers around in a short time and I have to thank him on this place. I came to already built cold steel body (first day we mount the pulsed nozzle on) and in few days we get first reasonable images on HBr photodissociation. Analysis of the clustering conditions in the pulsed nozzle results into our first publication [1]. More important, it shows that after minor improvements the developed system AIM (Apparatus for IMaging) is suitable of independent operation in cluster mode. It triggered further research project on AIM concerning acetylene clusters [2]. The last project on CFC dissociation dynamics was led by Viktorya Poterya and I act only like technical support [3].

In 2011, together with acetylene photodissociation experiments I started to explore the CluB (Cluster Beam) experimental system, which is the headstone of our group. The replacement of existing low field TOF with photofragment ion imaging was second planned step in the imaging implementation in our laboratory. Except the detection part I used the design of Juraj from the AIM apparatus and successively test the CluB VMI replacement on HBr molecular system. Here I must thank to all the group members supporting me during this step since the work on CluB setup was completely new experience. At the end of the

year subsequent problems with laser system resulted into switch of our focus on neutral molecule - cluster collisions [4]. I joined Jozef Lengyel in the study, further exploring the continuous molecular beam source and associated analyzing techniques.

The funds from AVCR in 2011 allowed us to purchase new mass spectrometer, its selection and adaptation on specific conditions of our experiment was particularly in my competence. The choice is custom built double stage bipolar reflectron time of flight mass spectrometer with varaible energy electron gun realized by S. Kaesdorf company in Muenchen. The scientific program of 2012 was dictated by the delivery of the spectrometer and consecutive problems with laser system. We focused fully on the TOF implementation. Work together with Jozef progress fast and we were able to prepare particular mass spectra for wider publication on HNO_3-water coagulation [5]. Simultaneously we conducted the research on acetylene [6] which forms the end chapter of the thesis.

The work is structured into four main chapters and introduction. In the Introduction, motivation to study processes in clusters is sketched together with main effects of solvent on molecular reactions in clusters. Objectives of the thesis are then defined in separate section.

The first chapter gives introduction to the photofragment imaging technique. It is divided into several parts identifying the method in wider context of photodissociation dynamics studies, describing its historical evolution as well as the particular approach applied in our laboratory. Last part of the first chapter explains the term angular distribution of photofragments, an important observable of photofragment ion imaging technique.

The second chapter focus on AIM experiment. Experiment as well as the basic measurement procedures are exhibited on HBr case study. The chapter aims to be a good reference for future members starting their work on the setup.

Third chapter is devoted to the experiments on the CLUB experimental setup. Similar to the previous chapter we try to provide a tutorial style description to photodissociation experiments with size selected clusters as well to the newly implemented TOF technique.

Fourth chapter is devoted to acetylene chemistry in clusters. It is a compilation of three papers published on theme introduced in short overview.

In summary, there are three new experimental schemes working in the lab which demonstrate significant experimental efforts. However, the building stages are usually not so productive in the view of modern science evaluation methodology. This is reflected also in the structure of the thesis.

Introduction

Last years we are bombarded with the word nano from each side. Nanoparticles can be found in wash detergents, colors, fabrics... Nanoparticles are used in catalysis, and are extensively studied for medicine applications like drug delivery or cancer treatment [7, 8]. A typical way people think about nanoparticles is that nanoparticles are small particles of bulk or liquid providing a huge surface to volume ratio and remaining its original properties. However, the properties are kept only down to dimensions of tenths of nanometers. At smaller dimensions both physical and chemical properties significantly change (see e.g. [9]). Bright examples of the change are studies of phase transitions performed on a variety of nanoparticle systems [10, 11, 12]. Small nanoparticles in a size range above dimers up to several hundred atoms or molecules are called clusters. Clusters are particles in which surface layer of the particle dictates its behavior [13]. Scientists from various fields are now interested in clusters due to "nano trend". The miniaturization driven by possible applications requires deep knowledge of property change at nanoscales.

The thesis sails around the nano trend to more essential questions. A main motivation is an understanding of complex chemical processes on fundamental level. Studies of homogeneous clusters for example provide us basic information on weak interactions between neutral molecules like Van der Waals or hydrogen bond (e.g. [14, 15, 16]). Studies of heterogeneous clusters are now on the best way to illuminate the fundamental processes in atmospheres or living organisms (e.g. [17]). An important advantage is that in many cases the studies are supported by theory. Clusters of several molecules are on the limit of current ab initio computational methods which are not applicable to larger systems. Consequently, the experiments with clusters provide important benchmark for theory (e.g. [18]).

There are several ways to study clusters. Techniques like STM or AFM microscopy are often used in surface science to study merely conducting clusters. Similar, clusters prepared in colloids are restricted to crystallizing species. Additionaly, it is impossible to eliminate the influence of substrate or solvent in any of the mentioned techniques. Question rise up if there is a way to overpass the restrictions. Thanks to the developement of molecular beam technique we know the satisfactory answer. The observation of clusters in molecular beams by Becker [19, 20] gives us the chance to study free clusters by vacuum restricted techniques. Photofragment ion imaging and mass spectrometry are two examples

of such techniques discussed in the thesis. The molecular beam technique also allows us to vary the cluster properties by changing the expansion conditions. Cluster composition, size and to some extent temperature can be controlled in the molecular beam experiments, as it is demonstrated within the thesis.

The thesis presents studies of free clusters in vacuum with the main objective in mind - to explain the solvent effects on the reaction dynamics of molecules and clusters. We use lasers like universal tools to initialize photodissociation reaction which can be written in simplified form:

$$\mathrm{ABC}+h\nu \rightarrow \mathrm{ABC}^* \rightarrow \mathrm{AB}+\mathrm{C} \tag{1}$$

Photodissociation is often referred to as the half reaction since the dissociative excited state (ABC*) could be prepared in a bimolecular collision of appropriate precursors. Direct relations exists also to other dissociative processes like dissociative electron attachement, dissociative recombination or collision induced dissociation [21, 22, 23]. Therefore the results have general importance for molecular and cluster chemistry in solvent. The studies of photoinduced processes are complemented by studies of electron induced processes using new TOF spectrometer implemented within the thesis. The additional technique allows us to further explore a solvent role in chemical reactions. Examples of solvent effects are:

1. CAGING

Molecule inside the cluster is enclosed or caged by solvent. The effect of a cage on photodissociation dynamics was extensively studied in rare gas matrices (see e.g. [24]). The effect is usually explained from a mechanistic point of view, when dissociation products are slowed down in collisions with solvent. Photodissociation of molecules inside the clusters then results into KED (kinetic energy distribution) spectrum of fragments dominated by zero energy peak due to the kinetic energy loss in inelastic collisions with solvent.

Study in our group [25] shows interesting case of the caging behavior leading to significantly accelerated fragments. The behavior can be explained from a quantum mechanical point of view. Molecule in the solvent cage is no more in vacuum and therefore its dissociation limit is influenced by solvent. The solvent induced shift can completely close the dissociation pathway. The result is preferential quenching of molecule into highly vibrationaly excited ground state, like demonstrated on Fig. 1. Such way a vibrationaly hot precursor molecules are

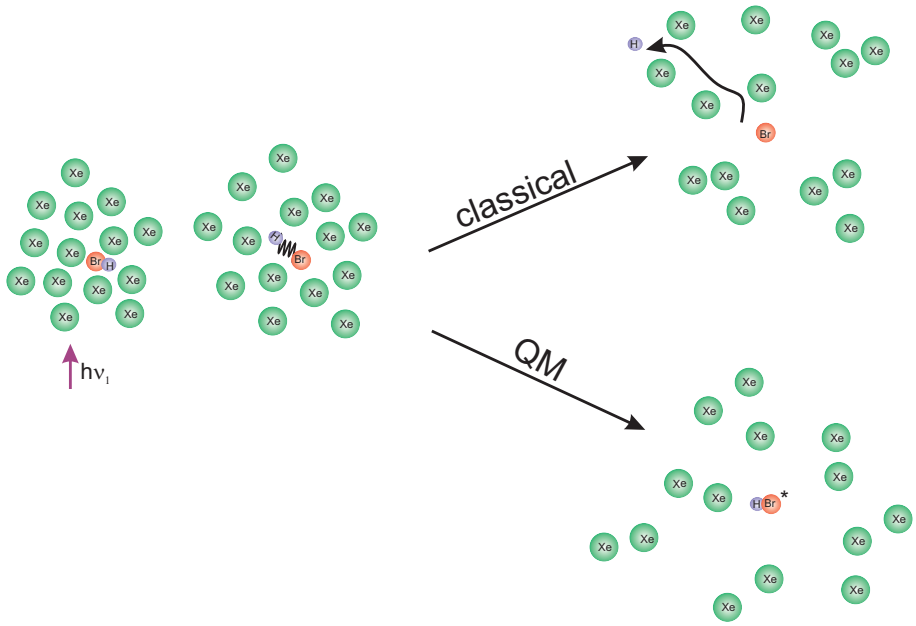

Figure 1: Two example scenarios of the cage effect. In classical case photodissociation products leave the cage, losing the kinetic energy in inelastic collisions with solvent. In quantum mechanical case solvent influence the dissociative electronic state closing the dissociation channel - excited molecule is formed

formed. In contrast to the classical view of dissociation followed by recombination driven by interaction between fragments the process is caused purely by solvent and can be viewed like quantum mechanical cage (or potential well) preventing the dissociation. Subsequent photon absorption can led to the dissociation of hot molecules and observation of the fast fragments in KED spectra.

The implementation of new photofragment ion imaging technique results into first full angular dependence study of both classical and QM caging phenomena. The studied systems were HBr in large rare gas clusters [1] (attachment 1)and acetylene clusters [2](attachment 3) respectively.

2. ENERGY TRANSFER

The number of molecules or atoms in a cluster provide a huge reservoir of energy. On one side the cluster can absorb significant amount of energy into its degrees of freedom or kinetic energy of evaporating constituents. This way reaction products are stabilized, excited precursor states are quenched or cluster constituents are excited. On the other side by an excitation or ionization of one of the cluster constituents we open a way to transform internal energy of molecules. The most striking example of energy transformation is the cluster ion polymerization process [26]. In a particular case of acetylene the cluster ionization results into

formation of variety of covalently bound ions (e.g. [27, 28]). A necessary condition of the ion polymerization is that excess energy of the system is above the energetic barriers separating the Van der Waals and covelently bonded ions [29]. We try to explain the energetics of the cluster ion polymerization process in the work which is a part of the thesis [6](attachment 5).

Getting back to the first case where cluster acts like energy sink, we should get back to the caging effect. In the work on acetylene [25] Farnik shows that observation of photofragments from vibrationally hot acetylene molecules is restricted to only short times after the absorption of first photon by cluster. At times above 0.5 ns the fragments are not observed and ground state molecule signal is enhanced. Process is sketched on Fig. 2. At short timescales electronically excited molecule quenches into the highly vibrationally excited ground state. At longer timescales vibrational relaxation proceeds via energy transfer to the solvent, resulting in cold molecule in ground state.

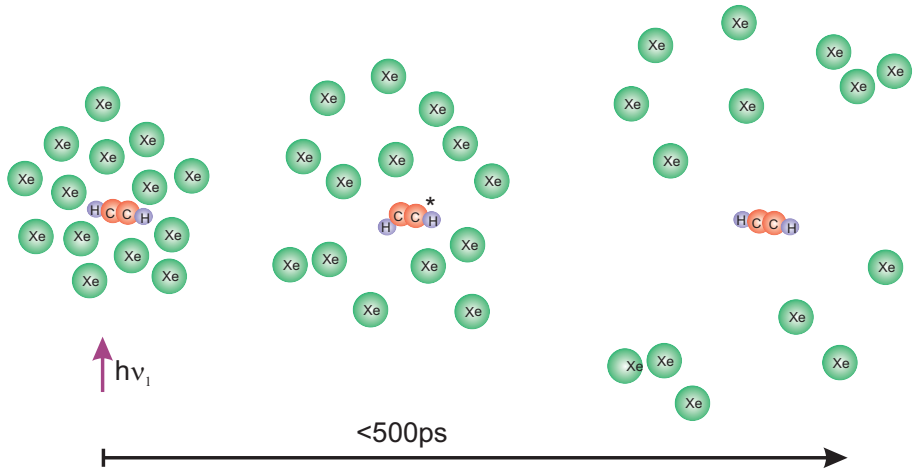

Figure 2: On the energy flow within a solvent. At times under 500ps after excitation fast fragments are produced from vibrationally hot molecules. At longer times products from vibrationally cold molecule dominate the spectra.

One of breakthroughs in understanding of energy transfer in solvent - time resolved spectroscopic study of a vibrational energy flow after the hydrogen transfer reaction [30, 31] shows the suitability of cluster approach to study solution effects. The references show that on short time scales interaction between hydrogen and donor molecule within the solvent cage dominates while on long timescales the reaction product is stabilized by interaction with solvent. The behavior is analogous to the two energy transfer mechanisms observed in clusters, as discussed in previous paragraph.

3. REACTANT

A solvent can often act like reactant. The "QM caging" mentioned above can be viewed like reaction between the molecule and solvent, since electronic states of both are involved. In this part we are interested in an opposite interaction resulting into opening of new reaction channels. Of course the first reaction coming into mind in solution is acidic dissociation. In our laboratory we focus on the dissociation of halogen halides, like already mentioned HBr or HCl. These are of high importance for atmospheric chemistry. The experiments with the halogen halides deposited on the surface of ice clusters [32, 33] show acidic dissociation similar to liquid phase. The dissociation predicted by [34] results into formation of halogen anion and hydronium cation. The UV light in stratosphere then promotes so called charge transfer to solvent (CCTS) excited state, when electron is transferred to hydronium and water molecule is stabilized by hydrogen ejection (see Fig. 3). Since energy of CTTS state is lower in comparison to dissociation limit of particular halogen halides, halogen radicals are formed at higher wavelengths in comparison to gas phase. Such red shift can result into significant radical yield increase in the Stratosphere. New TOF mass spectrometer implemented on CLUB experimental setup within the thesis was used to reveal the acidic dissociation in mixed HNO_3/H_2O clusters. The experiments show evidence of 4 water molecule minimum for HNO_3 solvent induced dissociation.

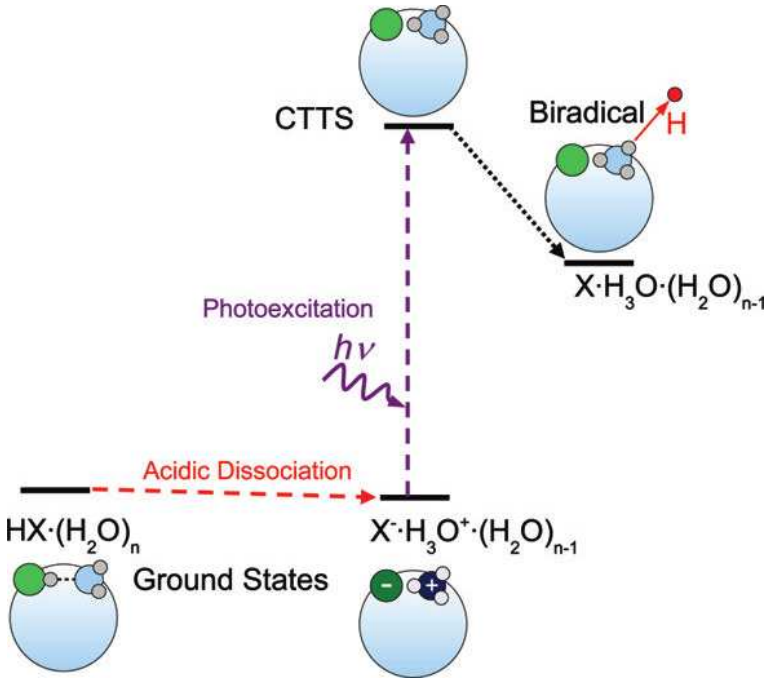

Figure 3: Cl radical formation after HCl acidic dissociation on the surface of ice nanoparticle. Adapted from [33]

So far we discuss the reactivity of solvent in the ground state. The important group of reactions are reactions involving excited or ionized solvent molecules. The example could be soft ionization of water clusters like observed by [35]. A synchrotron radiation tuned on Ar excitation energy results into formation of pure water cluster ions in contrast to protonated water clusters formed after near threshold electron or photoionization of water clusters. The ionization was explained to proceed via exciton transfer from Ar to low lying autoionization states of water clusters. Since it is well known that the the OH radical abstraction occurs after the ionization of water due to huge difference between water dimer neutral and ion ground states, it is clear that exciton transfer is not enough to describe the observation. There should be energy flow channel stabilizing the water clusters after ionization. To illuminate the process we use new TOF mass spectrometer with variable energy electron source, like it is described in chapter 3.

Clusters can influence the chemistry in many other ways. A cluster can collect and store reactive species or it can act like a catalyzer of reactions on its surface. There is an important role of surface layer influencing the chemistry from deposition to reactions and many other issues, which have not been discussed. We will not focus on these issues within the thesis, however we can touch some of them in following chapters due to complexity of the processes in clusters.

Objectives and Deliverables

An ultimate scientific goal of the thesis is to illuminate environmental effects on chemistry at nanoscale. Within the thesis we focus on solvent effects on photon and electron induced chemistry.

The title of thesis indicates its experimental character. A main experimental goal of the thesis is the implementation of photofragment ion imaging technique in our laboratory to study photochemistry in free clusters and nanoparticles. The technique allows to measure full angular distributions of photofragments, which was not easy to realize by previously used TOF technique (actually the kind of measurement has never been done on original setup). Additionally the technique was expected to improve the sensitivity of our photofragment kinetic energy measurements.

Implementation of the photofragment ion imaging proceeded in two steps. At first a new molecular beam experiment AIM (Apparatus for IMaging) was built to test a new photofragment ion imaging system in VMI (velocity map imaging) configuration. The tested system was expected to replace the low field time

of flight at our Cluster Beam (CLUB) apparatus. Test measurements on AIM shown that it is well suited for experiments with clusters and therefore AIM was used in several other experiments. Another VMI system was proposed to replace the low field time of flight spectrometer on CLUB apparatus. Additionally, a new system was proposed for mass analysis on CLUB apparatus. An aim was to implement these systems on CLUB and test them. The test phase dominated by experiments with HBr molecule and clusters was followed by main research phase dominated by experiments with acetylene molecule and clusters. The particular goals are listed as follows:

1. *Finish the development and test the photofragment ion imaging system (AIM).*
   - **a** Perform test measurements on HBr molecule.
   - **b** Continue experiments on photodissociation dynamics of acetylene clusters.
   - **c** Train colleagues on new experimental technique and support them during the experiments with CF_2Cl_2 in clusters.
2. *Design a new photofragment imaging system, replacing the low field TOF at CluB.*
   - **a** Perform test measurements on HBr molecule.
3. *Select and customize TOF mass spectrometer for CLUB system.*
   - **a** Perform test measurements on H_2O/HNO_3 clusters.
   - **b** Continue experiments on acetylene clusters.

A main goal of the written part of the thesis is to provide an introduction to the new techniques available in the lab. It aims to be a good reference and starting point for new colleagues coming to the lab. Thesis omit a repetition of already published results, rather some of the publications are attached. The research part of the work was described in the following publications:

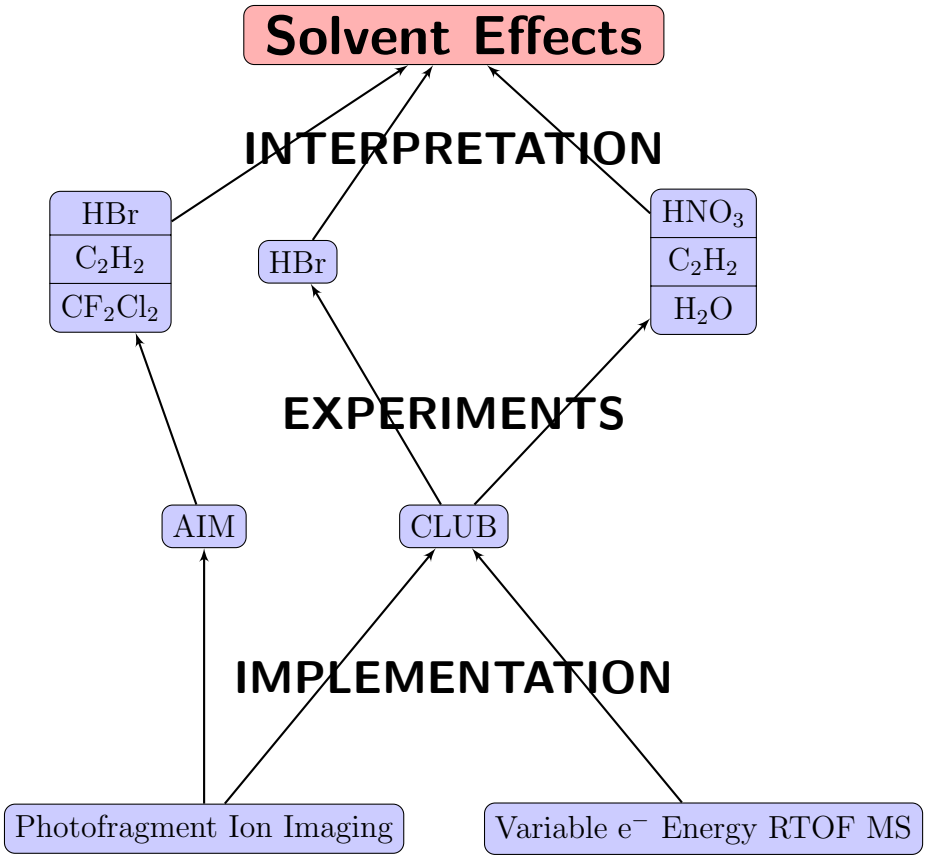

Figure 4: Logical bottom - up chart of the objectives in the thesis. Techniques newly implemented on CLUB and AIM experimental setups were used to study particular systems to reach the ultimate goal - illuminate the solvent effects on e^- and photon induced chemistry

Impact journals:

1a *Velocity map imaging of HBr photodissociation in large rare gas clusters [1]*; attachment 1

1b *Short review on the acetylene photochemistry in clusters: photofragment caging and reactivity [2]*; attachment 3

1c *Caging of Cl atom from photodissociation of CF2Cl2 in clusters [3]*; attachment 2

3a *Nucleation of Mixed Nitric Acid-Water Ice Nanoparticles in Molecular Beams that Starts with a HNO_3 Molecule [5]*

3b *Ionization of large homogeneous and heterogeneous clusters generated in acetylene−Ar expansions: Cluster ion polymerization [6]*; attachment 5

Week of Doctoral Students proceedings:

1b *UV Photodissociation of Acetylene in Various Environments[36]*; attachment 4

2a *Benzene Cation from Acetylene Clusters - Precursor of PAHs in Space[37]*

3b *From gas phase to bulk? Photodissociation of neutral size selected HBr_n clusters.*[38]

During the studies author participate on the following publications affiliated to the Charles University in Prague, which are not directly related to the thesis:

* *Dissociative electron attachment to the silane derivatives trichlorovinylsilane (SiCl3C2H3), tetravinylsilane (Si(C2H3)(4)) and trimethylvinylsilane (Si(CH3)(3)C2H3)[39]*
* *Electron Ionization of Dimethylphenylsilane - Appearance Energies of Selected Ionic Fragments[40]*
* *Uptake of atmospheric molecules by ice nanoparticles: Pickup cross sections [4]*

1. Ion Imaging in Photodissociation Dynaimcs

An interaction of light with matter is one of the most important energy transformation channels in Universe. Probably the most important result of the first experiments exploring an interaction of light with matter was an observation of exponential intensity decay. The Beer-Lambert exponential law is extensively used till nowadays in wide spectra of physical and chemical disciplines. The law provides a macroscopic description of absorption, which is the most important prerequisite of the photodissociation process. Nowadays, thanks to a developement of quantum theory we can see the absorption from microscopic point of view, like interaction of photon electromagnetic field with electrons in atom or molecule.

In our laboratory, we are focused on light induced processes in nature, specifically on Earth. A photon energy distribution of the emission of Sun can be approximated by Planck's law with black body temperature $\sim$ 5800 K. The distribution starts at $\sim$ 200 nm (5 eV), peaks in visible 500 nm ($\sim$ 2.5 eV) and ends by long tail in infrared region above $\sim$ 1000 nm ($<$ 1.2 eV). In the mentioned energy range (under ionization limit) photons can trigger a variety of processes. Some of the processes are shown on Fig. 1.1 together with the absorption spectra of hypothetical molecule XY. For example, we can see that discrete vibrational structure in the low energy part of the specra is followed by a continuous peak representing a transition into dissociative state. Absorption spectroscopy provide us the information about the first step in photodissociation reaction - energetics of dissociative excited state. In particular case of bound states it is possible to estimate also the upper limit for a bond dissociation energy using Birge - Sponer extrapolation [41]. However, we know nothing about the dissociation pathway - photodissociation dynamics.

To explore the photodissociation dynamics we should look on the second part of equation 1 - dissociation event. Rewriting the equation into form:

$$\mathrm{ABC(E_0)} + h\nu \rightarrow \mathrm{ABC^*(E_0} + h\nu) \rightarrow \mathrm{AB(E}_{el,vib,rot,kin}) + C(E_{el,kin}) + D_0 \qquad (1.1)$$

We have included bond dissociation energy D_0, internal energies of fragments and their translational energies. The energies represents dissipation channels for primary excitation event. Information about the energy redistribution is there-

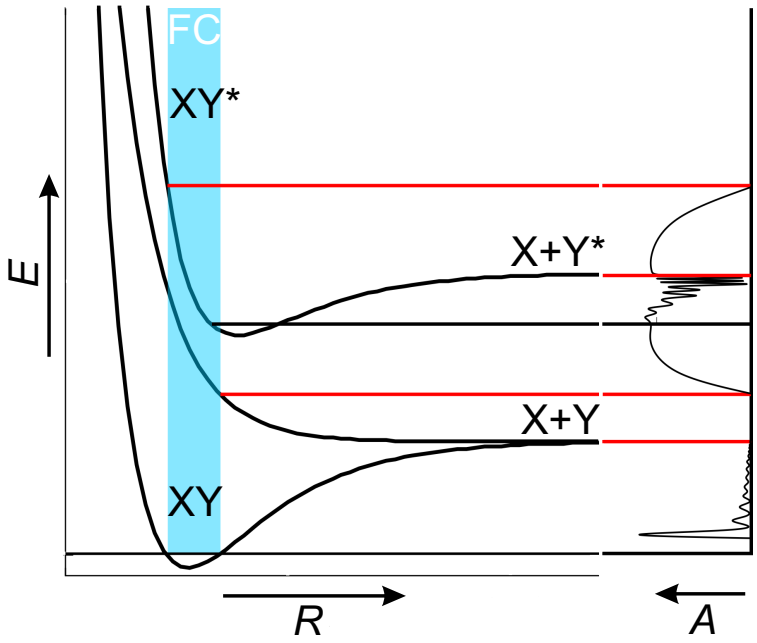

Figure 1.1: Potential energy curves of a hypothetical molecule XY and its absorption spectra.

fore second part of the photodissociation dynamics puzzle. The information can be obtained from complementary techniques based on determination of internal energies of photofragments (chemiluminiscence, Laser induced fluorescence) or kinetic energy determination of photofragments using translational spectroscopy techniques (translational spectroscopy, like presented within thesis). We wrote complementary techniques, since the techniques based on fragment emission are restricted to excited fragments and translational spectroscopy techniques are usually used to study fragments in the ground state.

A significant amount of knowledge about photodissociation event can be gained from vector correlations [42]. Therefore, angular distribution of photofragments provide us another important information. There are several ways dissociative potential energy surfaces can cross within the molecule [43] and assignment of excited to dissociative states is not always straightforward. The relation between excited and dissociative states is well described by transition dipole moment, which geometrical part is in direct correlation to angular distribution of photofragments. The angular distribution of photofragments can help us to make an estimate of dissociative state lifetime too. In case the dissociative state lifetime is long, the angular distribution is usually smeared by rotational movement of the excited molecule.

The final step to full understanding of the photodissociation dynamics is the addition of time domain into the experiments. Now it is possible to study time

evolution of all the mentioned parameters step by step in femtosecond pump - probe experiments. In the next subsection we will look on the time evolution of photofragment ion imaging technique in more details.

1.1 Historical Overview

Without a doubt the birth of modern photodissociation dynamic studies is dated to 1960s due to the invention of novel light sources - LASERS [44, 45]. Lasers provide high intensity and spectral brightness not approachable with any light sources used previously.

Discussion about photodissociation dynamic experiments should be started by the article of R.N.Zare and D. Herschbach [46]. The article from 1960s presents relations between transition dipole moments, angular distribution of photofragments and their correlation to emission from excited fragments. Article is fundamental for development of photodissociation dynamic techniques based on fluorescence or laser induced fluorescence of photofragments [47]. More important in the context of photofragment ion imaging approach, the work triggers several breaking works in the field starting with the first use of position sensitive detector by Solomon in 1967 [48]. Solomon studied photodissociation of iodine and bromine molecules by polarized light from mercury vapor lamp. Photofragments were detected on thin film tellurium hemisphere. The tellurium "detector" preparation makes the technique a bit inconvenient and the formation of tellurium-halogen complexes during long measurements reduce the conclusiveness of the experiments. Even worse, the technique requires specific thin film for each particular fragment [49]. The photodissociation dynamics therefore waits for another impulse which came in the form of universal detection technique - ionization by electrons.

In the year when Lee and Herschbach introduced the electron ionization technique in molecular beam scattering experiments [50] Wilson introduced the technique in photodissociation experiments [51]. A photodissociation dynamics technique based on a measurement of the photodissociation fragment velocity by time of flight (TOF) from photodissocaition region to the ionization region of quadrupole mass spectrometer take name translational or recoil [52] spectroscopy. A drawback of the technique was in low sensitivity due to an angular discrimination of the detected photofragments and a low precision due to uncertainities in determination of ionization point and quadrupole flight times. The way to avoid the problems comes in the form of Resonance Enhanced Multiphoton Ionization

technique - REMPI. REMPI allows laser ionization of products immediately after the dissociation and with a high efficiency. It is based on the observation of significant enhancement of ion signal after multiphoton ionization once the energy of any particular step is in resonance with excited state of the precursor molecule. It was observed already in first multiphoton ionization MPI studies in 1970's (e.g. [53]). Important property of REMPI process is its selectivity. Tuning the laser frequency on the energy of electronic transition of specific fragment or transition from specific vibrational state, only the ion yield of particular precursor is enhanced. In 1977 Zare performed first studies on reaction dynamics of Ba+HCl using MPI detection of BaCl [54].

In 1980s REMPI advanced rapidly allowing its routine use for methyl radical detection in famous CH_3I photodissociation study of Houston and Chandler [55]. In the experiment CH_3I in pulsed molecular beam was dissociated by 266nm NdYAG laser and CH_3 photofragment was ionized by 2+1 REMPI at 330nm. An influence of the ionization (outgoing electron) on a speed of photodissociation fragments is negligible, therefore the formed ion cloud reflects the velocity distribution of dissociating fragments. CH_3^+ ions were accelerated to the detector via series of grids including mass gate eliminating the signal from other ions formed by nonresonant multiphoton ionization. Detector configuration consisting of multichannel plate converting the ion signal into electrons and further intensifying it and phosphor converting the electron signal into fluorescent light is used in photofragment ion imaging till nowadays. Phosphorescent light was detected by polaroid film or Reticon diode array. The result was 2D image of CH_3 ion distribution - the first photofragment ion image. Since then ion imaging method pass expansive evolution and utilizes in plenty of laboratories studying reaction dynamics. The progress was mapped in several publications [56, 57, 58] therefore we will mention only the most important developments already implemented in our lab or perspective improvements.

In our experiments we are using photofragment ion imaging optics in VMI (Velocity Map Imaging) configuration. The upgrade of Eppink and Parker [59] is based on the ion optics simplification in a way that ions are focused spatially, resulting in their divergence in velocity space. It is simple consequence of phase-space conservation described by Liouvilles theorem. The VMI ion optics consist of three simple lenses without grids. The design provides effective focusing system as well as elimination of problems connected to grids, like loss of ions on wires or image distortions.

In the photofragment ion imaging, 3D cloud of dissociating fragments is de-

tected on 2D position sensitive detector. To reveal the information about the true distribution of photofragments we have to perform back projection of the 2D circle into 3D sphere. Cut through central part of the backtransformed sphere is then used for further analysis. There are several ways to perform back projection. The simplest approach used in our laboratory is the inverse Abel transform. More sophisticated backprojection methods include onion peeling [60] or BAsis Set EXpansions (BASEX) [61]. The methods are well compared in the chapter 3 of ref. [57].

There is an experimental way to avoid complicated post processing. It has been named slice imaging [62]. Slice imaging is based on the selective detection of the central "slice" of the expanding photofragment cloud. Increasing the ratio between the expanding photofragment cloud diameter and slice thickness we get into good approximation to the central cut obtained using backtransformation methods mentioned in previous paragraph. The biggest advantage of the slicing is that it is unrestricted to any symmetry requirements of expanding photofragment cloud, which are necessary during backprojection. Several slice imaging approaches were developed so far and are well described in publication [56].

The term "slice imaging" was first used by Geberhardt for complicated pulsed photofragmen ion imaging scheme [62]. The extraction is pulsed with extraction pulse delayed with respect to the REMPI photofragment ionization pulse. This way the cloud of photodissociating fragments expands in the field free region. Extracted photofragment ion cloud is then detected on a detector in significantly prolonged time. By pulsing the detector, central slice of the prolonged photofragment cloud can be obtained. Rising the extraction delay, the cloud can expand more and the ratio between cloud length ($\rightarrow$ tof peak width) and slice width ($\rightarrow$ detection pulse width) can be enhanced. However, zero field during the extraction requires grid design (to shield the penetrating field from rest of electrodes) and it is also sensitive to the shielding of the ionization region, like will be discussed in chapter 2.

Easy alternative to slice imaging is the DC slice imaging developed in A. Suits group [63]. It is based on low extraction field allowing the expansion during longer flight time. Additional ion optics plate then focus the cloud perpendicular to the detector, what results into defocusing (or prolonging) the cloud in the direction of the detector axis. Prolonged cloud can be once again cut by pulsing the detector. Same DC slicing idea was applied also by Lin et al. [64] using different electrode configuration.

One of the interesting applications of photofragment ion imaging is the imag-

ing of vibrationally mediated photodissociation [65, 66]. Technique is based on vibrational excitation of precursor molecules followed by photofragment ion imaging study. This way the details of energy transfer in multiatom molecules can be revealed. However, the VMP have even more important application. Similar to REMPI the first resonant step makes it strongly selective. The ability of the method to study precursor with specific vibrational mode was succesively used by Reisler group (see e.g. [67, 15]) to study small clusters. The vibrational levels are slightly shifted in dimers or higher oligomers due to neighboring molecules. Therefore in the first step of VMP it is possible to resonantly excite vibration of molecule in cluster of specific size. The sophisticated neutral cluster size selection was flavored with REMPI detection of neutral water molecules in recent study of small water clusters [68, 15, 69]. The VMP start with excitation of specfic hydrogen bonded OH stretch within dimer (3602 cm^{-1}) and trimer (3536 cm^{-1}) molecules followed by REMPI of water. The analysis of VMI images results into most precise experimantal values of dissociation energy of small water clusters $D_0((H_2O)_3) = 2650 \pm 150$ cm^{-1} $D_0((H_2O)_2) = 1105 \pm 10$ cm^{-1}. The tunable IR OPO laser system recently purchased to our group gives a promise of similar exciting experiments in near future.

1.2 Photofragment Ion Imaging Experiment

Let's summarize a typical photofragment ion imaging experiment. Simple sketch of the configuration is depicted on Fig. 1.2 a). We want to explore the dynamics of photodissociation reaction by study of the dynamics of photodissociating fragments. The name of the technique nicely guide us through particular steps in photofragment ion imaging:

1. PHOTOFRAGMENT We get the studied molecule into vacuum by means of molecular beam. This way we significantly cool its degrees of freedom down to several rotational levels. Then a photodissociation reaction is initialized in vacuum by excitation of molecules by laser light. The excitation energy is redistributed according to the equation 1.1. The excitation is dipole transition induced by interaction with laser electric field and therefore we are selectively exciting the molecules with transition dipole moment in the direction of electric field. The selective excitation results into anisotropic distribution of fragments. However, the anisotropy can be smeared by rotations of excited state and therefore depends strongly on its lifetime. In the first step a **cloud of photofragments is formed**.

2. ION In second step **the cloud** of neutral photofragments **is ionized**.

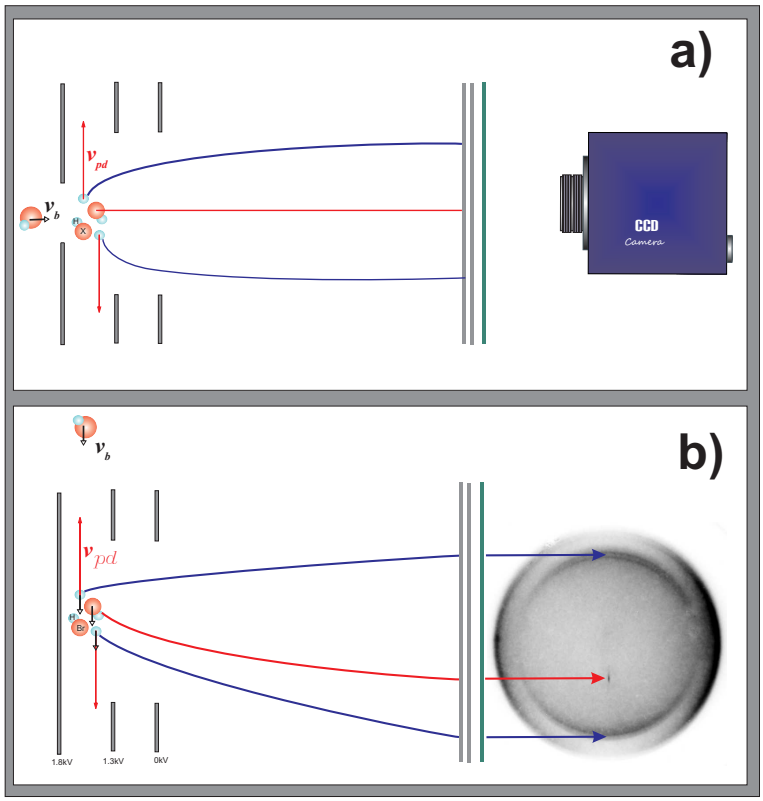

Figure 1.2: Sketch of the direct VMI configuration a) and orthogonal VMI configuration, as it is used in our experiments (b)

Usually, REMPI ioniztion is used. Resonant character of the process results into significant enhancement of the signal from particular photofragment in comparison to nonresonant multiphoton ionization of another constituents present in reaction region. The kinetic energies of fragments in the ionization step are influenced only by recoil kick of outgoing electron at levels $\sqrt{m_e/m_m}$ which is negligible. **Ions are** then **extracted** towards the detector. In VMI configuration fragments with the same velocity vector are focused onto the same spot on the ion imaging detector.

3. IMAGING Imaging step of the 2D projection of the 3D velocity distribution formed by fragments hitting the detector starts with signal conversion to electrons. The electron signal is amplified in multichannel plate(s)and electrons are accelerated onto the phosphor covered glass inducing the phosporescence. Electrons are converted to light which is then captured by digital camera converting the light back to electric signal.[1]. A digital two dimensional projection **image of photofragment distribution in velocity space is obtained**. 2D image is then analyzed to obtain information about true photofragment distribution in

[1]There are several novel types of position sensitive detectors reducing the number of conversion steps and therefore obtaining better time resolution see e.g. www.roentdek.com

velocity space.

1.3 Perpendicular Velocity Map Imaging

In our experiment, we are restricted to the orientation of VMI detector perpendicular to the molecular beam axis. Lets discuss advantages and disadvantages of the configuration.

In ideal molecular beam experiment all the energy of the expanding gas is transformed into the motion of expanding particles in the direction of the molecular beam. Energy conservation then results into simple formula for mean speed in the direction of the molecular beam:

$$< v >= \sqrt{\frac{2Cp * k * T_0}{M * u}}$$

The value of $< v >$ for atomic gases is in good agreement with prediction due to exclusively translational temperature cooling. The situation is more complicated in the case of molecular gases due to the fact that cooling of internal degrees of freedom not always follow the entropy decrease. Situation becomes even more complicated once the phase transitions and clustering comes into the focus, as will be discussed in the following chapters. Often the expansions are made only with small impurities of a studied molecule in the buffer atomic gas to keep the buffer gas conditions. The $< v >$ trend for mixture is depicted on Fig. 1.3). We can see that $< v >$ is not high in comparison to the typical speeds of dissociating fragments(see e.g. Tab. 2.4). However, most of photodissociation experiments avoid to deal with $< v >$ by orienting the molecular beam towards the detector. Such "standard" orientation of VMI system in the direction of molecular beam is depicted on Fig. 1.2 a) On Fig. 1.2 b) is the configuration used in our experiment - "perpendicular".

In standard orientation of VMI molecular beam passes through a hole in the VMI stack towards the detector. The influence of beam velocity $< v >$ vanish since the beam is parallel with VMI axis and tuning of the experiment is significantly simplified (molecular beam is already positioned in the center of VMI ion optics). The configuration allows much shorter distances between the nozzle and reaction region. Therefore, higher sensitivity can be achieved in standard configuration. The configuration is well suited for high resolution and low intensity measurements. On the other hand the central - low velocity part

Table 1.1: Parameters in Eq. 1.2

Cp atoms	Cp diatomics	Cp polyatomics
$\frac{5}{3}$	$\frac{7}{5}$	$\frac{9}{3}$
mixture a%A in B	Cp=a*Cp_A +(100−a)*Cp_B	
	M=a∗M_A +(100−a)∗M_B	
u=1.66053892×$10^{-27}kg$		
k= $\frac{R}{Na}$ =$\frac{8.314462175JK^{-1}mol^{-1}}{6.0221415\times10^{23}mol^{-1}}$ =1.3806488×10^{-23}m^{2}kg s^{-2} K^{-1}		

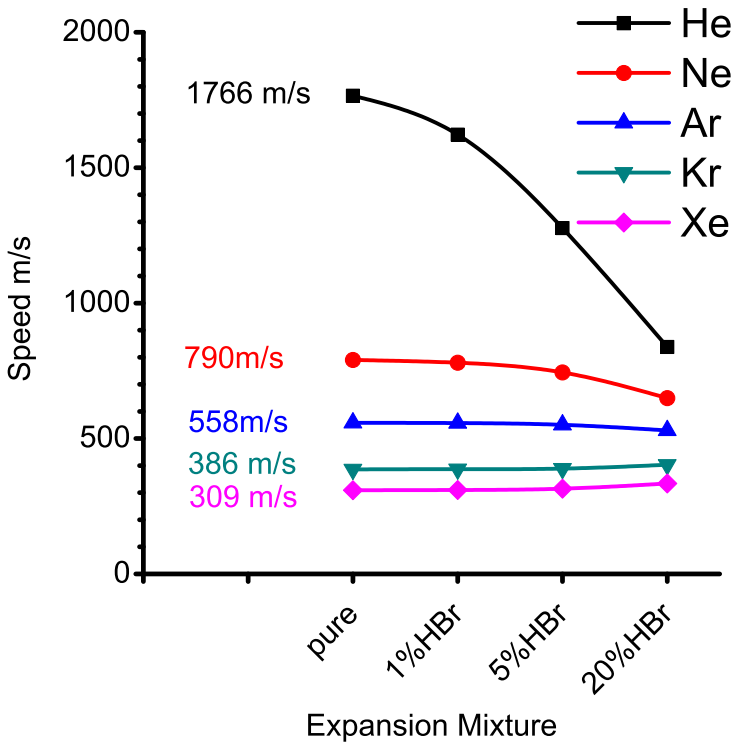

Figure 1.3: Mean speed $< v >$ of molecules in molecular beam expansions of various gases and effects of HBr admixture (according to eq. 1.2).

of an image can not be analyzed due to high signals from multiphoton ionized parent ions and neutrals from the molecular beam. This way significant amount of information is lost about the low energy part of the spectra and molecular beam properties. In the Introduction we already mentioned that the most pronounced cluster effect on photodissociation is the caging which results into fragments with near zero kinetic energies. Loss of the low energy part of the spectra in standard configuration VMI makes it inapplicable for cluster studies.

In perpendicular orientation of the VMI we have to deal with neutral beam speed influence on the image and more complicated tuning procedure. Also the distance from the nozzle and consequently concentration in the beam is significantly lower. However, in our particular case there are much more advantages of

the perpendicular configuration. At first a molecular beam can pass through the VMI unperturbed and can be analyzed by other techniques.[2] In cluster experiments (see e.g. [70]) it is important also because of high intensities and energies of the neutral beam, which can saturate or destroy the MCP detector.

The perpendicular configuration is used especially in experiments in which the beam information is crucial for the experiment, like e.g. reactive scattering experiments[71]. The information about the beam velocity can be interesting also in photodissociation studies, especially at conditions when clustering can occur (see e.g. [72, 1]). Most important for our experiment is the fact that it is possible to study central low energy part of the photodissociation image without any influence of the neutral beam or parent ions. Simply, each fragment is shifted on the detector differently due to same velocity of precursor $< v >$ and different flight times, as it is depicted on Fig. 1.2. Another type of experiments with position sensitive dsetectors placed perpendiculary to the molecular beam axis are so called reaction microscopes [73]. Recently the reaction microscope concept was improved significantly by single detector coincidence imaging developed in the group of M. Janssen [74, 75].

We should stress that using the VMI in perpendicular configuration provides the full information about the produced ion cloud in contrast to the standard configuration. This was crucial for the setup development within the thesis.

1.4 Angular Distribution of Photofragments

We already mentioned that angular distribution of photofragments can provide us important information about correlation between states. The well known formula based on derivation of Zare and Herschbach [46] describes the angular distribution of photofragments like:

$$I(\theta) = \frac{\sigma}{4\pi}[1 + \beta P_2(\cos\theta)],$$

where $P_2(\cos\theta)$ is second legendre polynomial of $\cos\theta$ and β is the only free parameter characterizing the distribution. The exact classical or quantum mechanical derivation can be found in several works (e.g. [76, 77, 78]). Here we mention

[2]Now it is possible to buy MCP detectors with hole in the central part of the detector, allowing the beam passing through VMI in configuration parallel to the molecular beam axis. (see e.g.http://baspik.org) However their performance, especially the gain uniformity is rather low.

only few important ideas behind which can help to understand the "technical" estimation elsewhere.

Easiest quantum mechanical approach to photoabsorption is semiclassical. The classical electromagnetic field $\vec{\mathbf{E}}(t)$ is integrated like small perturbation of the system, described by perturbation hamiltonian [3]:

$$H'(t) = \vec{\boldsymbol{\mu}}.\vec{\mathbf{E}}(t)$$

The probability for transition between two electronic states is then:

$$P = \frac{1}{\hbar} \mid \vec{\boldsymbol{\mu}}.\vec{\mathbf{e}} \mid^2 E^2(\omega),$$

where we extract the electric field polarization vector $\vec{\mathbf{e}}$. Apparent is the angular dependence of the dot product of the electric field polarization vector with transition dipole moment $\vec{\boldsymbol{\mu}}.\vec{\mathbf{e}}$. Integrating the cosine angular $\vec{\boldsymbol{\mu}}.\vec{\mathbf{e}}$ dependence through all molecule orientations and assuming that transition dipole moment is vector with parallel or perpendicular orientation to the molecular axis we end up with equation 1.3. (see ref. [46, 76] for details)

However the picture is significant simplification of reality. There are several factors influencing the distribution of photofragments. Main influence is due to rotation of the molecule, its excited state and photoframents. Their involvement requires the treatment of transition through transition dipole operator T. The transition dipole moment can be expressed like the matrix of elements of type:

$$\vec{\boldsymbol{\mu}_{ab}} = < \psi_b \mid e\mathbf{r} \mid \psi_{\mathbf{a}} >$$

Where $\mathbf{r}$ is simply the displacement operator. In optimal set of coordinates such displacement can be treated like rotation connected to the corresponding change in angular momentum. [4]. Since rotation is purely geometrical transformation of coordinates quite complex questions can be answered through "simple" goniometry. Angular momentum theory additionally shows that even in the case of more

[3] At wavelengths typical for photodissociation - hunderds of nanometers, we can neglect the magnetic field component and also the position variation of electroomagnetic field (dipole approximation).

[4] see nice example in [79] chapter 11.2 page 348

complex operators (e.g. transition moment dipole of multiphoton or nonadiabatic transition) the geometrical part of the operator can be extracted. [5] The disentanglement of rotational and nonrotational (in ref. [76] called physical) part of operator is expressed by Wigner-Eckart theorem:

$$< \alpha' j' m' | T_q^K | \alpha j m >= (-1)^{j'-m'} \begin{pmatrix} j' & K & j \\ -m' & q & m \end{pmatrix} < \alpha' j' || T^K || \alpha j >$$

Theorem simply extracts the 3j symbol fully describing the rotational(geometric part). Lets assume dipole transition, T_q^1. From the definition of 3j symbols only states with q=-1,0,1 are possible. Therefore, only the transitions leaving the dipole projection on the axis of quantization unchanged (parallel transition) or changing it by +/-1 are possible (perpendicular transition). Angular momentum approach significantly simplifies the transformation between molecule-fixed and space-fixed frames in case of accurate derivations of angular distribution of photofragments. Derivation details are well described in cited publications [77, 78] and accurate results have more theoretical than experimental importance. However there are two modifications of expression 1.3 which are extensively used.

The first modification is the formula for the dissociation of state selected molecules. It has form [80, 81]:

$$I(\theta, \phi) = \frac{\sigma}{4\pi} P_{JKM}(\cos\theta)[1 + \beta P_2(\cos\theta)]$$

State selected molecules can have specific orientation in respect to the direction of laser polarization in the molecular frame $P_{JKM}\theta_m$ before the photodissociation what results into the additional $P_{JKM}(\cos\theta)$ term in the expression. Since $P_{JKM}(\cos\theta)$ can be once again expressed in the form of legendre polynomials [6] we can expect additional structures in the angular distribution of photofragments obtained from photodissociation images.

The second modification of eq. 1.3 is the formula for multiphoton processes.

[5] For all operators behaving under rotation as follows:

$$\mathbf{r}\mathbf{T}^{\mathbf{K}}_{\mathbf{q}}\mathbf{r} = \sum_{\mathbf{q}'} \mathbf{D}^{\mathbf{K}}_{\mathbf{q}'\mathbf{q}}(\mathbf{r})\mathbf{T}^{\mathbf{K}}_{\mathbf{q}'}$$

see [76] for details.

[6] see e.g. expression 21 in ref. [80] or ref. [81]

It has form:

$$I(\theta,\phi) = \frac{\sigma}{4\pi}[1 + \beta_2 P_2(\cos\theta) + \beta_4 P_4(\cos\theta) + ... + \beta_{2n} P_{2n}(\cos\theta)]$$

The higher order polynomials does not effect the angular distribution significantly in case of one laser processes. However, in pump - probe experiments where the polarization of the lasers can be changed, such higher order terms can provide additional information about photodissociation process (see e.g. [82, 83]). Example is the evaluation of nonadiabatic transition probabilities for HBr molecule [84]. Good introductory text is that of Brown [85]. In cited works β parameter in laboratory frame is expressed using anisotropy parameters for particular polarizable fragments in molecular frame $a_q^K(p)$ where p is the transition symmetry (parallel, perpendicular, mixed). This way the probe influence is disentangled and observed distribution is directly linked to physical processes in molecular frame.

Through text we frequently used the β parameter characterizing an angular distribution of photofragments. There are few significant values of β fullfiling the equation 1.3. They are β =2 β =-1 and β =0 corresponding to purely parallel transition, purely perpendicular transition and isotropic distribution, respectively. A mix of contributions from different transitions then results into β in between these values, like in mentioned work of Rakitzis [84] or like will be discussed in the chapter 2. Another significant value can be found for the angle θ. At $\theta = 54.7°$ second order legendre polynomial is equal to zero. The fact was often used in low field TOF experiments with polarization set at "magic" angle 54.7° (see e.g. ref. [86]).

2. Experiments on AIM

AIM - apparatus for imaging is simple experimental setup, which combines pulsed molecular beam source with velocity map imaging. AIM was built to test VMI before its mounting on main - CLUB experimental setup. Now it is used independently to study both molecular and cluster photodissociation dynamics in perpendicular VMI configuration. Advantages of the perpendicular configuration were discussed in previous text.

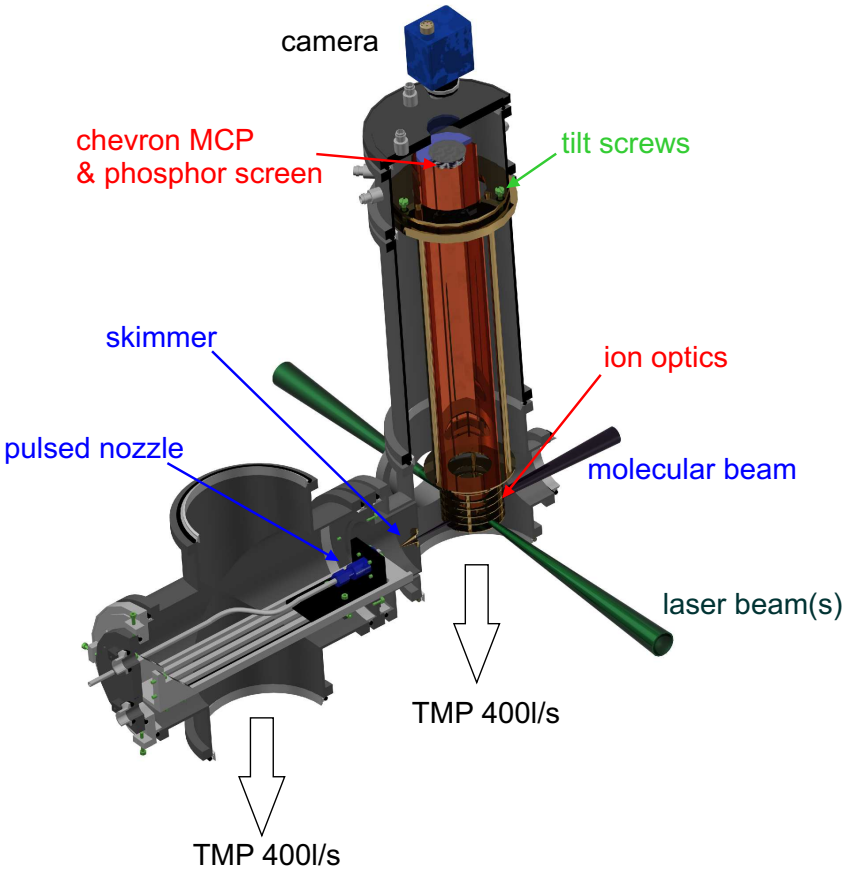

Figure 2.1: Model of AIM experimental setup.

The artistic view on vacuum part of experimental setup is on the Fig. 2.1. Schematics of whole apparatus is on fig. 2.2. The setup consist of two differentially pumped vacuum chambers - source chamber in which molecular beam is formed and VMI chamber in which photodissociation is studied. During the design and further modification, the compactness and mobility of the system was kept in mind. Now the vacuum system including pumps have length 105 cm width 40 cm and height 160 cm (210 cm with camera). All the electronics including computer is in standard 23 in rack. The mobile design allows use of AIM on the light sources

outside the laboratory. In the laboratory UV light from dye or excimer lasers is used to prepare excited states and probe photofragments. Through chapter individual parts of the experimental setup are explained. Then the experiment tuning and measurement procedure is presented on HBr photodissociation case study.

2.1 Inlet and Molecular Beam Source

The molecular beam source is based on KF150 cross piece originally evacuated by 280 l Varian diffusion pump. It has been replaced by Pfeiffer 400 l turbomolecular pump improving the purity of the vacuum and the compactness of the setup. Additionally, air cooling is sufficient during operation, increasing the mobility of the setup in contrast to external water cooling required for the diffusion pump. The base pressure in the chamber is $\sim$5x10^{-7} mbar and typical pressures during operation are $\sim$7x10^{-6} mbar to $\sim$2x10^{-5} mbar.

Sample is prepared by mixing the expansion gas with studied molecule in high pressure inlet system build from Swagelok components. Molecular beam is formed by expanding the gas mixture through electromechanical General Valve pulsed nozzle (see fig. 2.2 for inlet details).

The nozzle is driven by home build electronic cirquit. It was built by Ondrej Votava and it is based on 74LS221 single shot driving circuit in combination with BD437 power switching transistor. 74LS221 integrated cirquit could be triggered by external TTL pulses or internal LM555 timer. Pulse length is controlled by ln2xRxC combination of 0.1 μF capacitor and 5 kΩ resistor + 100 kΩ potentiometer, resulting in theoretical pulse width range 0.35 ms - 7.3 ms. Maximum pulse voltage is 40 V. Commercially available driving circuits are operating in two step pulse regime where short high voltage (280 V) pulse opens the valve and low voltage 10 V keeps it open till the remaining time of pulse. [1]

Therefore in the commercially available driving circuits the opening time is shortened in comparison to a low voltage pulse and the coil overheating risk is reduced in comparison to a single high voltage pulse. The setting for opening part of pulse can be as low as 5 μs, however the mechanical properties of push/pull springs results to typical times required for full opening $\sim$180 μs. (The importance of full nozzle opening in cluster experiments will be discussed elsewhere.) It means that the limit of $\sim$500 μs achievable using single pulse in our experiment is of comparable length. Additionally the millisecond opening times are sufficient for operation with 10 Hz laser systems in the lab.

Normally the nozzle is operated at the maximum pulse voltage to lower the open-

[1] Well known is e.g. Iota One driving cirquit http://www.smijapan.com/PDF/Iota$_O ne_M anual_R ev_C .pdf$

ing time and pulse width is adjusted to the experimental requirements. The expanding channel of the nozzle is 0.5 mm in diameter and 5 mm long. Nozzle is mounted on movable stage fully adjustable from outside the vacuum. Horizontal and vertical directions could be changed by simple sliding of the mount flange on the O-ring seal. Nozzle to skimmer distance is adjustable by leadscrew on the rotational feedthrough.

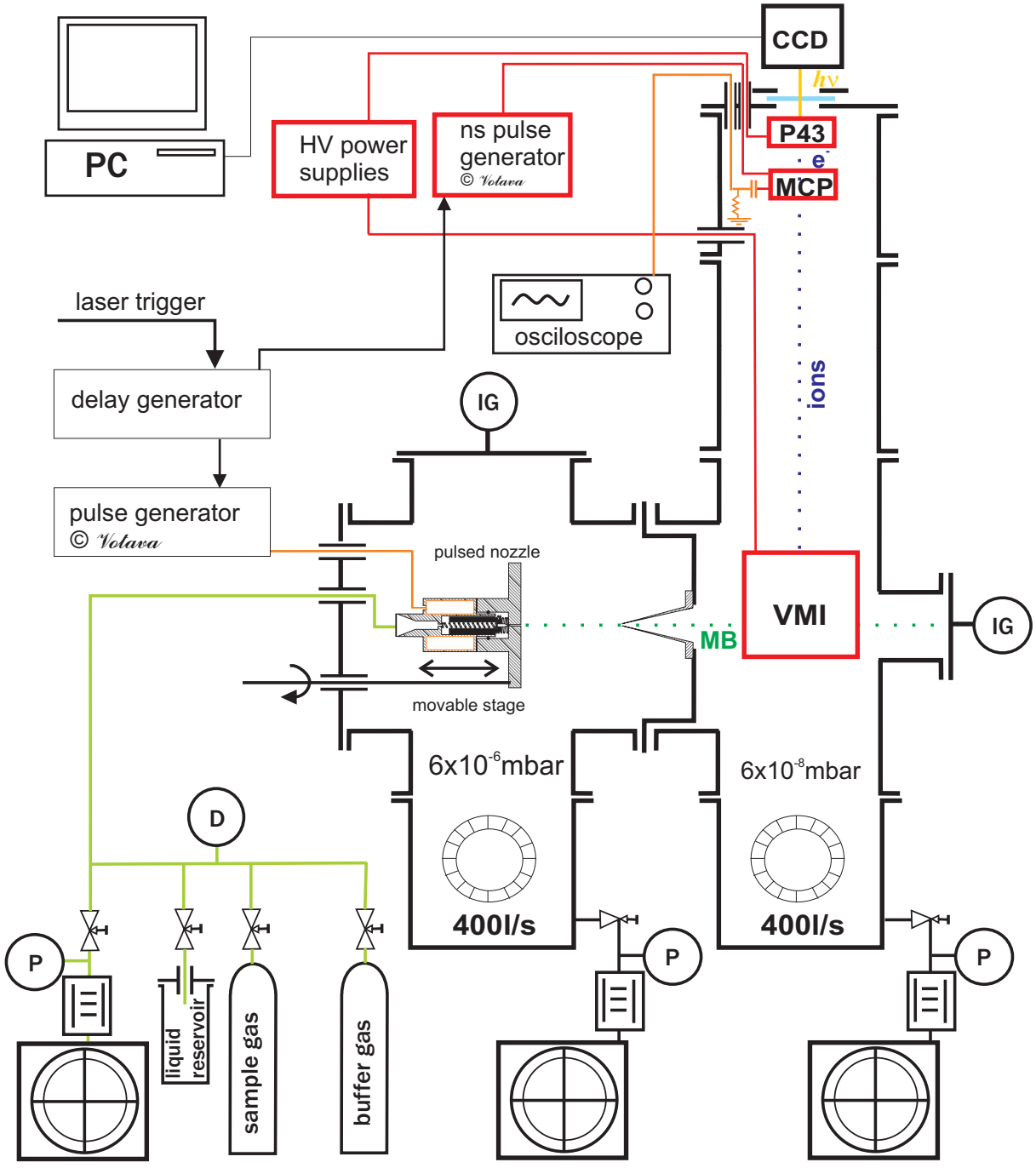

Figure 2.2: Schema of AIM experimental setup.

2.2 Imaging Part

The photofragment ion imaging part consist of VMI ion optics according to Eppink and Parker [59], aditional lens for image sizing, TOF tube, and position sensitive detector.

All the electrodes of VMI hold on stainless steel ring in upper part of the system (see Fig. 2.1). The ring is lying on stainless steel holder fasten to vacuum collar, which incorporates also the high voltage feedthroughs for ion optics. This way all the system can be removed from the vacuum chamber without disconnecting. Between the holder and the ring there are 6 screws allowing tilting of the ion optics with respect to the rest of vacuum chamber and detector. It is used during the alignment procedure. The alignment procedure is as follows:

At first the vertical position of the reaction region with respect to the expected crossing point of laser and molecular beam is set by screws which connect the ion optics and TOF parts. The adjustment is performed outside the vacuum chamber.

The next step is performed with ion optics mounted on vacuum chamber. Diode alignment laser is used to visualize expected molecular and laser beam paths. The tilting screws on ring holder are then used to center the VMI reaction region to the beam crossing. To do so we are using simple "beam tool". It is lying on extractor electrode during the alignment procedure showing the center of the laser interaction region. After the coarse alignment of the ion optics the chamber is closed by flange which holds the position sensitive detector system.

Position sensitive detector was custom built at IESL (The Institute of Electronic Structure and Lasers), Crete. It consist of two TOPAG microchannel plates (MCPs) in chevron configuration amplifying the ion signal followed by Proxivision P43 phosphor screen emitting the light detected by CCD camera.

MCPs are 50(47) mm outer(active) diameter with channel diameter 15 μm and channel distance 18 μm. Maximum sustainable voltage is 2.2 kV and gain is $\sim 10^6$. The MCP electron signal can be collected from the backplate floating on the high voltage by measurement of the voltage on a capacitor discharge resitor (primitive capacitively copuled current - voltage converter). The electronic signal is then displayed on the osciloscope and provide us the important information about the time domain in our experiment (e.g. TOF mass spectra). The rest of information is gained from the image obtained by accelerating the electrons on the Proxivision phosphor screen.

On the phosphor screen, electrons are converted to phosphorescent light. The phosphor screen is a borosilicate glass plate covered by P43 phosphor (Gd2O2S:Tb). The P43 phosphor is emitting at $\sim$ 545 nm (green) with the conversion efficiency depending on the energy of electrons. The conversion efficiency has maximum of 600 photons/electron around 10 kV. However, maximum voltages which could be applied to standard phosphor plates without special coatings are $\sim$ 6 kV with efficiency 500 pho-

tons/electron. On AIM experiment we are using the voltages in range 3 kV to 4 kV (240 photons/electron to 360 photons/electron). The decay time of the P43 phosphor is in ms range sufficient for our experiments. [2]

The light emitted from the phosphor screen pass through the vacuum view-port and it is detected outside the vacuum. The intensity of light is enough to be visible by eye. Therefore, there are no special requirements on image detection system.

On AIM we are using standard Unibrain monochrome CCD camera to detect the image. Monochrome CCD sensors are better suited for P43 light detection due to higher sensitivity in green in comparison color sensors. Camera is positioned on support 30cm above the viewport due to minimum focus distance of the used objective. The light path between vacuum viewport and camera is shielded by PVC tube covered by black tape to prevent background signals from light sources in laboratory. Digital image is transferred to computer via 1394a interface. The image acquisition is controlled by LabView programme developed at IESL, Crete. Postprocessing is done in ImageMan program developed by Juraj Fedor.

We already know that ionization at REMPI wavelength is highly selective. However it is still 3 photon process for hydrogen and significant laser intensities are required, which can result into nonresonant multiphoton ionization. To get rid of ions produced in nonresonant processes it is good to select the ions of interest by pulsing the MCP detector. By pulsing the detector ions are selected according to their time of flight and therefore mass to charge ratio. The pulsing is realized on the first MCP plate. During the mass selected measurements front plate is at 0 V and backplate at 1.2 kV. The 1.2 kV acceleration voltage is not sufficient to detect the ions. At specific time of flight for particular ion front plate is pulsed to - 300 V, total MCP voltage rise to standard 1.5 kV and ions are detected. The negative pulse on front plate during the detection have not only the advantage in low pulsing voltages but also in a further noise reduction (see e.g [87]). The pulse generator for mass gate was built by Ondrej Votava and is based on the design of Geberhardt [62].

2.3 Laser System

Several laser systems in the lab provide us with wide range of wavelengths ranging from ArF UV at 193 nm to IR OPO in far infrared. Selected wavelengths we come to contact through the thesis are listed in Tab. 2.1. Since the principle and operation of particular laser sources is well documented in monographs and operating manuals, we will pass through the lasers fast and we will focus more on the alignment procedure of the VMI. We used three laser systems on AIM setup. The laser systems are pulsed with 10 Hz repetition frequency and a typical pulse length in is nanosecond range.

[2] in applications requiring faster detection P47 phosphor (Y2SiO5:Ce,Tb) can be used with decay times 100ns or even more sophisticated materials, see e.g.http://www.crytur.cz

Table 2.1: Around the LAB wavelengths TAB

laser	wavelength nm	energy eV	comment
NdYAG	1064	1.165	fundamental
	532	2.33	2nd harmonics
	355	3.49	3rd harmonics
	266	4.66	4th harmonics
DYE	610-650	2.03-1.9	DCM range in ethanol
	635-675	1.95-1.84	DCM range in DMSO
	460-500	2.69-2.48	Coumarin 480 range
	243.135	5.099	REMPI Hydrogen
	235.336	5.268	REMPI Cl
	235.205	5.271	REMPI Cl*
ArF	193.3	6.4	

The first system is 243 nm UV light source used for REMPI ionization of hydrogen. It is Laser Analytical Systems LDS205 tunable dye laser pumped by second harmonics of Quanta Ray GCR Pro 2.5 J NdYAG nanosecond laser. Dye output is processed in Quanta ray *WEX*II wavelength extender. Two KD*P crystals are used in *WEX* to first double the dye laser output 630 nm and then mix it with NdYAG fundamental resulting in radiation ∼243 nm. In *WEX* the temperature variation of crystal properties is compensated by series of servo motors rotating the crystals. The compensation results into good stability of the beam during long measurements. Additionally, the described method of wavelength preparation, which is called mixing after doubling is principally suited for measurements requiring long stability. The suitability is based on the long lifetime of used dyes pumped by visible light (e.g. DCM). On the other hand the mixing after doubling method is not well suited for large changes in wavelengths due to sensitivity of used crystals and complicated adjusting procedure. System is therefore used exclusively for REMPI ionization of hydrogen. For tuning in wide range of wavelengths we recently purchased second dye laser combination, which is based on simple frequency doubling of dye laser output.

The second laser system consist of FineAdjustment Pulsare dye laser pumped by Innolas SpitLight 1500 NdYAG. The dye laser is pumped by third harmonics of NdYAG, which allows us to use blue dyes (e.g. coumarines). The output of the dye laser ∼480 nm is then doubled in BBO crystal integrated in the laser system. The doubling results into required UV radiation. In thesis it was used for REMPI detection of hydrogen and chlorine fragments. An advantage of the system is easy exchange between the REMPI wavelengths, on the other hand the used blue dyes degrade fast resulting in intensity variation in long experiments. Typical working periods with coumarins were 1-2 days (5 l of mixture) in comparison to ∼month with 0.5 l DCM mixture on old mixing after doubling system.

Third laser system used in the lab is ArF excimer Lambda Physik COMPEX. It is

discharge based excimer laser with beam profile in centimeter dimensions. Produced 193 nm is the shortest wavelength actually available in the laboratory. It is used for the primary excitation in photodissociation experiment ("pump"). The light at ∼193 nm is already absorbed in air, therefore there is significant decrease in the laser intensity with path length. Most important is the absorption of oxygen well known Schuman-Runge system resulting in the effective ozone formation [88]. Additionally, the laser intensity is attenuated in optical components (e.g thin film polarizer reduces the intensity 10x) and vacuum viewports. The intensity of the laser in the experiment therefore significantly differs of the value measured on the laser output and must be estimated.

Laser Intensity

At first step laser power before and after the vacuum chamber is measured P_{in}[mJ/pulse] and P_{out}[mJ/pulse] respectively. After the transmission of vacuum windows is computed according to:

$$T = \sqrt{\frac{P_{out} - P_0}{P_{in} - P_0}}$$

We used P_0[mJ] for background light intensity measured by power meter out of the laser beam. We also expect that both windows have same transmission (therefore $T*T$). In the next step power passing into the reaction region is computed like $P_r = P_{in} * T$. Highest influence on the true number of interacting photons have the size of the laser spot in the interaction region. Therefore it is convenient to use laser intensities in units of W/cm^2 or photons/cm^{2}s^{-1}. To do so we have to estimate the focused laser spot size. The correct way is to use the beam waist parameter. Beam waist $2w0$ is the minimum diameter of the Gaussian beam focus spot and can be calculated according to:

$$w0 = \lambda . \frac{2f}{\pi . D}$$

The laser spot area is then $s_{w0} = \pi . w0^2$ and intensity of the laser $I_{w0} = P_r / s_{w0}$. The beam waist works only for well defined Gaussian beam (e.g. dye laser beam in Tab. 2.2) For the lasers with poor beam profile (e.g. excimer laser in Tab. 2.2) it is better to use simple geometrical approach.

Geometrical calculation is based on diameters of two beam profiles measured after the focusing lens, their distances and distance to the focus point. Trigonometry of similar triangles is then used to calculate the spot area s_g and intensity I_g. Intensitiy values for dye and excimer laser are listed in Tab. 2.2 together with the parameters used for the calculation.

Table 2.2: Intensity calculation for lasers with different beam characteristics. In the case of dye laser the beam profile is Gaussian and beam waist parameter can be used. In the case of excimer laser the beam is not so well defined and it is better to use geometrical spot size.

laser (λ)	P_0 [mJ]	P_{in} [mJ/pulse]	P_{out} [mJ/pulse]	T	P_r [mJ/pulse]	pulse width[ns]	F [mm]	D [mm]	$w0$ [cm]
Dye(243nm)	0.05	2.55	0.38	0.36	0.8	5	500	9	$8.594\text{x}10^{-6}$
ArF(193nm)	0.055	1.423	0.542	0.59	0.849	25	500	26	$2.36x10^{-6}$

s_{w0} [cm^2]	s_g [cm^2]	I_{w0} [W.cm^{-2}]	I_g [W.cm^{-2}]	photon energy [J]	I_g [$\text{photon.s}^{-1}\text{.cm}^{-2}$]
$2.32\text{x}10^{-6}$	$2.5\text{x}10^{-6}$	$6.89\text{x}10^{10}$	$6.3\text{x}10^{10}$	$8.175\text{x}10^{-19}$	$7.7\text{x}10^{28}$
$1.75\text{x}10^{-7}$	$4.7\text{x}10^{-6}$	$1.94\text{x}10^{11}$	$7.2\text{x}10^{9}$	$1.029\text{x}10^{-18}$	$7\text{x}10^{27}$

Laser − VMI Alignment

An alignment of the system starts with prealignment of the laser into the chamber. Removable crosshairs on inlet and outlet fused silica windows are used during prealignment. Precision tuning is then performed on VMI images.

Before we can use the VMI image for laser position tuning we have to ensure that camera is focused on the phosphor screen. For this purpose we use the laser to dissociate and ionize background gas in evacuated chamber. The REMPI ionization is effective and so there is always some background we can detect. We turn on the VMI voltages. Typical operating voltages in VMI mode are 1.8 kV on repeller and 1.36 kV on extractor and rise the voltages on MCP and phosphor. At first phosphor voltage is raised to 2 kV to prevent field emission from phosphor to MCP and then MCP voltage is slowly raised in 500 V steps up to 1.5 kV. After rising the phosphor voltage to 3.2 kV - 3.5 kV the green spots from phosphor screen should be well recognized even by an eye. Then image acquisition is started and focus of the camera is changed to see the single spots. It is important, since there can be some reflection of light outside the vacuum which can look like the diffuse signal. Then the objective is focused to minimize the single spot size.

In next step we set the voltages into spatial map imaging mode (described on Fig. 2.3). To do that we need to set the extractor voltage above the repeller one, typical values in our experiment are U_{rep}= 1.8 kV and U_{extr}= 2 kV. This way we magnify the laser beam pathway through the reaction region. Working still on background we can precisely tune the laser horizontal position and focus.

In next step the molecular beam is inlet and signal is tuned on maximum on the oscilloscope by moving the nozzle position with respect to skimmer and changing the delay between the laser shot and nozzle opening pulse. Nozzle horizontal position can be fine tuned similar to the tuning of the laser focus. Laser vertical position is also tuned to reach the best overlap with molecular beam. Camera orientation can be also

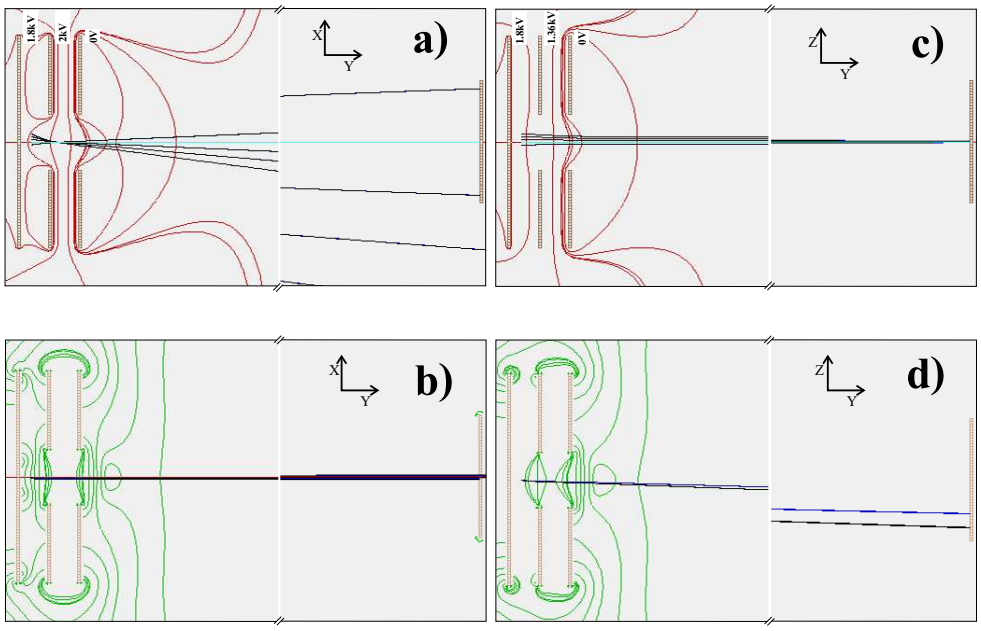

Figure 2.3: Two groups of protons from same positions in X direction (5 ions 1mm in distance around center) and two diferent kinetic energies (0.5eV an 1eV) are accelerated by ion optics in Spatial map imaging mode (a and b) and Velocity map imaging mode (c and d). (dimensions and values are similar to our experiment). We can see that in case of SMI the position of the ions are magnified since the energies are focused in VMI mode the energy difference is magnified since the positions are focused.

fine tuned in this stage. Abel transform used in post processing require symmetric image and it is better to align the camera parallel with laser beam than to rotate each image during the post processing. After the alignment procedure is finished, we can start measurement.

Usually, we are working with voltages on MCP ∼1.5 kV, reducing the single ion spot size and damage risk. Since only the signal of ions hitting the MCP are enhanced, MCP is noiseless amplifier. Therefore it will make more sense to go to higher voltages. The spot size can be then enhanced by higher voltage between the MCP and phosphor screen. Typically we are using values around 3.5 kV on phosphor due to problems with breakdowns in HV BNC feedthroughs (stated to 5 kV). Solving the problem (adding the SHV feedthrough for phosphor) can improve the spot brightness and sensitivity of the experiment. At first view it does not make much sense. Once we are converting the ion enough efficient to detect it, there is no reason to improve brightness. However the issue is connected to the dynamic range of measurement. Once, ions are detected with different intensities the averaging results into artificial decreasing of the intensity of low signal part and increasing of the high signal part. Additionally measurement is restricted to dynamic range of used camera. On the other hand in regime where all

ions are detected with maximum intensity we are restricted only by length of summing and stability of our experiment. The second regime is usually called ion counting [89]. Of course the choice of regime depends on the system studied. In the high intensity experiments like HBr photodissociation described in following chapters it is reasonable to work in regime where image is obtained in few laser shots. At low intensities it is better to work in ion counting regime.

2.4 HBr Photodissociation

HBr molecule was chosen for the test measurements on the AIM apparatus. A main reason for the selection was a simplicity of the experiment. Both, photodissociation and hydrogen REMPI detection can be done within one laser shot at 243 nm due to broad absorption of HBr in the region [90]. HBr is also well known from plenty of previous studies. Both gas phase and cluster environment photodissociation dynamics studies were performed so far and will be discussed within the chapter.

Hydrogen bromide is heteronuclear diatomic gas. The basic parameters of the molecule are listed in Tab. 4.1. A main complication of experiments is a fact that HBr is quite toxic and highly corrosive gas. Experiments have to be care with special focus on safety. Additionally, special care must be given to inlet and roughing vacuum pumps.

Table 2.3: Selected properties of Hydrogen Bromide [91], [92], [93] [86]

Physical	mass	79.92617 (100)
		81.92412 (97.5)
		80.9125 (avg)
	melting point	186 K
	boiling point	206 K
	vapor pressure	2.308 MPa at 294 K
Energetics	Enthalpy of formation	- 36.29 kJ/mol
	Bond Strength	3.7456 eV (361.39 kJ/mol)
	Ionization energy	11.68 eV
	Vibrational quanta	2439 $cm^{-}1$ (0.3024 eV)
Structural	bond length	14.14 $\AA$
	dipole moment	0.78 D
Other	Odor threshold	$\sim$ 2 ppm
	Irritation of respiratory tract	$\sim$ 5 ppm

HBr is well suited for fundamental exploration of photodissociation dynamics in translation spectroscopy experiments. Possible excitation and energy dissipation channels are significantly reduced in comparison to polyatomic molecules and kinetic behavior of individual dissociating fragments could be well separated. Three main excited states can be accessed in the studied UV photon range between 6.5 eV and 5.1 eV. The

highest transition probability is to $A^1\Pi_1$ state which is fully allowed from $X^1\Sigma_0$ ground state. Two other states $a^3\Pi_1$ and $a^3\Pi_0$ can be accessesd due to spin orbit coupling, which strengthens with the size of halogen atom.

The excited states correlate into ground state Br($^2\Pi_{3/2}$) and Br*($^2\Pi_{1/2}$) excited state dissociation limits. The spin excited state form 14% of the total bromine signal [86]. Angular distribution of ground state Br($^2\Pi_{3/2}$) have purely perpendicular character while the β parameter of Br*($^2\Pi_{1/2}$) photofragment angular distribution depends strongly on photodissociation wavelength.

Sometimes [86, 94] the dissociation behavior is explained by Hund's coupling cases (see e.g [95]). Hund's cases represent reductions of quantum numbers to set of "good quantum numbers" for each particular Hund's case. The neglect of particular quantum numbers is based on the fact that the projections of the respective orbital(L), spin(S) or rotational(R) angular momenta on the internuclear axis $\vec{\mathbf{r}}$ (Λ, Σ, Ω respectively) vanishes for particular couplings. Except the easier computation, the concept allows to make the predictions for behavior in particular cases.

For hydrogen halides two Hund's cases are typical - case a) and case c). In the case a) L is strongly coupled to internuclear axis and S is coupled to L.[3] In such case we can expect that spin of the system will not change after photoexcitation what fits most of the diatomics. Due to low spin splitting of Fluorine atom HF fits well the Hund's case a). On the other side stands HI with large spin splitting fitting the description of Hund's case c). In Hund's case c) the spin orbit coupling (S − L) prevails that of L coupling to the internuclear axis.[4] In such case spin can change after photoexcitation.

The photofragment angular distributions usually fits the Hund's classification. HF is primarily excited into $A^1\Pi_1$ state via perpendicular transition and resulting photofragment distribution have $\beta = -1$ [96]. Larger hydrogen halides have larger spin orbit couplings resulting in more and more effective excitation of $a^3\Pi_1$ and $a^3\Pi_0$ states via parallel transitions. The photofragments are then detected with both $\beta = -1$ and $\beta = 2$ distributions.

However, not everything fits the simple Hund's approximation. The most pronounced discrepancy is in branching ratios between the ground and excited states of the halogen photofragments. By the way of example HF $A^1\Pi$ excited state correlates exclusively to F ground state dissociation limit but the observed branching ratio between excited state F* and ground state F photofragments at 193.3nm is 0.7 [96]. It is clear that even in so simple systems like hydrogen halides nonadiabatic transitions will play important role. In hydrogen halides it is directly connected to the fact that spin orbit coupling will change with internuclear distance.[5].

State of the art theoretical study on photodissociation of HBr molecule including

[3] $\Omega = \Lambda + \Sigma$

[4] $\Omega = \vec{\mathbf{r}}.(\mathbf{L} + \mathbf{S})$

[5] the relation is well described in the work of Nikitin Zare [97]

nonadiabatic effects was performed by Smolin and coworkers in 2006 [98]. The computation describes previously observed deviations ($\beta = -0.88$ vs. $\beta = -1$ see [84]) from ideal anisotropy parameter for Br($^2\Pi_{3/2}$) dissociation limit. The deviation is caused by $a^3\Pi_0$ state coupling to the $X^1\Sigma_0$ molecular ground state. The same coupling influences also the observed Br/Br* branching ratio. The strong variation of the β parameter for the excited Br*($^2\Pi_{1/2}$) photoproducts was described on the basis of nonadiabatic coupling of $A^1\Pi_1$ and $a^3\Pi_1$ states to the $t^3\Sigma_1$ state, which can not be accesed by direct excitation in UV region. Dependence of the mentioned couplings on the internuclear distance is on fig. 3 in cited work [98], which is good reference of HBr photodissociation dynamics in gas phase.

HBr photodissociation was extensively studied also in clusters. In principle all the solvent effects were already demonstrated on this simple molecule. At first photodissociatin of HBr clusters by 243 nm photons was studied by low field TOF technique in the group of Udo Buck [99]. Caging of photodissociation products was observed, which results into strong zero energy peak in kinetic energy distribution spectra of hydrogen photofragments. The zero energy feature was found to grow with the cluster size in good agreement with theoretical predictions of caging effect. In the follow up publication [100] autors reveal more details on angular distributions and branching ratios of the photofragments. The careful study results into observation of additional features in the kinetic energy ditribution spectra. The high energy features were attributed to originate from photodissociation of vibrationally excited precursor molecules. The vibrationally excited molecules were interpreted to form after collisions with outgoing H fragments. The effect was further observed in the mixed HBr-Rg clusters studied by low field TOF [101] and VMI within the presented thesis [1]. Studies of the single HBr deposited on the surface of large Rg clusters then illuminates the effect of orientation of the deposited molecule on the final velocity of photofragments [102]. The results of HBr cluster studies done in the group of U. Buck and mentioned within the paragraph are reviewed in ref. [103].

The effects were further explored in studies which combines experimental and theoretical approaches. In work [104] the effect of molecule orientation was further explored. More details on cluster preparation for orientation studies and interpretation of the intensities in between the main spectral features of KED spectra can be found in the work of Farnik [105]. The work [106] is then focused on molecular dynamics simulations to interpret the dependence of the caging effect on the cluster size for large Ne clusters.

In our group HBr photodissociation dynamics was studied in context of heterogeneous chemistry in atmospheres. Detailed study of the photochemistry on ice nanoparticles results into observation of the acidic dissociation of the HBr molecules on the surface of ice particles prior to the dissociation [107]. The mechanism of the follow up processes induced by photons was explained on the basis of quantum chemical calculation in the publication [32]. Recent study of HBr in rare gas clusters [1] is attached to

the thesis (attachment 1).

2.4.1 Measurement

We already discuss the VMI alignment and preparation for measurement in previous chapters. Here we focus on the measurement procedure. Measurement starts with tuning of VMI voltages on the parent ion spot. The parent ion signal reflects only velocity distribution of neutrals in the beam and therefore in ideal case it should be only a point. In reality it is rather oval due to speed diference in parallel and perpendicular directions of molecular beam. To enhance the parent ion signal and reduce the REMPI signal from hydrogen photoproduct ion we usually perform the tuning at wavelengths under the REMPI value. The goal of tuning procedure is to achieve as narrow and bright spot as possible. When the voltages are tuned we can start the measurement.

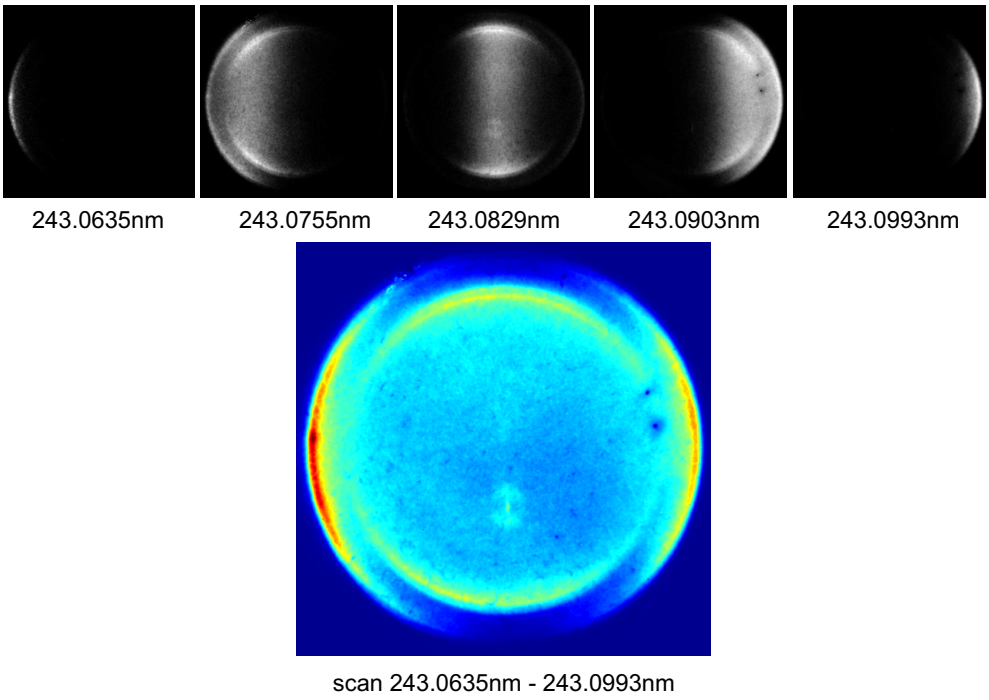

Figure 2.4: High speeds of fragments after photodissociation results into Doppler shift of their absorption. Therefore, fragments with different speeds are REMPI ionized at different wavelengths. Full velocity map image (color) is obtained as a sum of images at particular wavelengths.

As it is clear from name, REMPI is resonant process. Narrower linewidth of the laser tuned on the resonance enhance the signal more than the laser intensity spread through wide linewidth (only the photons in resonance are effective in the ionization process). However, after the dissociation fragments posses high velocities (in which we are interested), these velocities cause large Doppler shifts in comparison to laser linewidth. Fragments dissociating in the direction parallel with REMPI ionization laser will collide with photons at different energies (absorption line will be broadened).

The broadening of the absorption results into situation depicted on Fig. 2.4. To obtain full image of dissociating fragments with laser of reasonable linewidth we have to scan through whole Doppler profile. To obtain full velocity map image we sum the images taken at particular wavelengths. Raw data image is analyzed in the ImageMan software. Raw data represents 2D projection of 3 dimensional velocity distribution. To obtain information about original distribution we need to perform back transformation. Our transformation algorithm is based on the inverse Abel transform, which requires spherical symmetry of the dissociating fragment cloud in the velocity space. In first step we have to precisely center our image. Next step is Abel transform itself. The details of the particular procedures could be find in the ImageMan program manual. Information about the energetics and angular distribution of photofragments could be obtained from inverted image like discussed in following section.

2.4.2 TKER

The Abel transform and data processing always depends on the software used and is well explained in manuals to particular software. Here we pass through the data interpretation procedure with focus on energetics.

Table 2.4: TKER, kinetic energies and speeds of Hydrogen photofragments after photodissociation of HBr evaluated on the basis of the literature discussed in section 2.4

wavelength	Br state	TKER	H fragment kinetic energy	H fragment speed
243nm	Br	1.354	1.337	15999
	Br*	0.898	0.886	13024
193nm	Br	2.669	2.636	22464
	Br*	2.212	2.636	20452

The procedure is well demonstrated on Fig. 2.5. We already performed Abel transformation of the raw image (greyscale) obtaining the central cut through Newton sphere of dissociating fragments (color). By integrating the Abel transformed image through all angles we result in the velocity distribution of fragments, where velocity is in dimensions of pixel/TOF. To obtain the energy distribution we have to divide the intensities by velocity. [6] The v axis have to be transformed to energy. Since both pixel to meter and TOF to second transformations are linear, the simplest way is to perform transformation:$(pixel/TOF)^2.A = eV$ The transformation is then reduced to search for calibration constant A. In example we can use the values for HBr Tab. 2.4. We know that maximum in energy distribution represent ground state H+Br($^2\Pi_{3/2}$) and H+Br*($^2\Pi_{1/2}$) excited state dissociation limits. The slope of a linear fit to the dependence of local maximum position in $(pixel/TOF)^2$ dimensions to dissociation limit

[6] Distribution functions have to be normalized: $\int f(v)\,\mathrm{d}v = \int f(E)\,\mathrm{d}E \implies f(E) \sim \frac{f(v)}{v}$

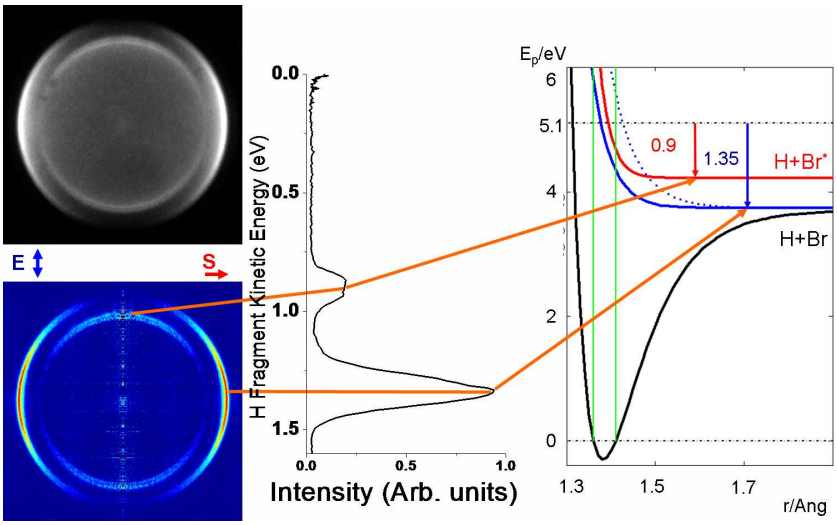

Figure 2.5: TKER information mining from VMI image in present experiment. Raw data (greyscale) are inverse Abel transformed (color) and intensities are integrated through all angles. Obtained velocity distribution is transformed into energy distribution for particular fragment. Estimated TKER can be correlated to particular reaction channels due to known photon energy in experiment.

values in eV is universal calibration constant, which holds for the particular fragment and VMI voltages.

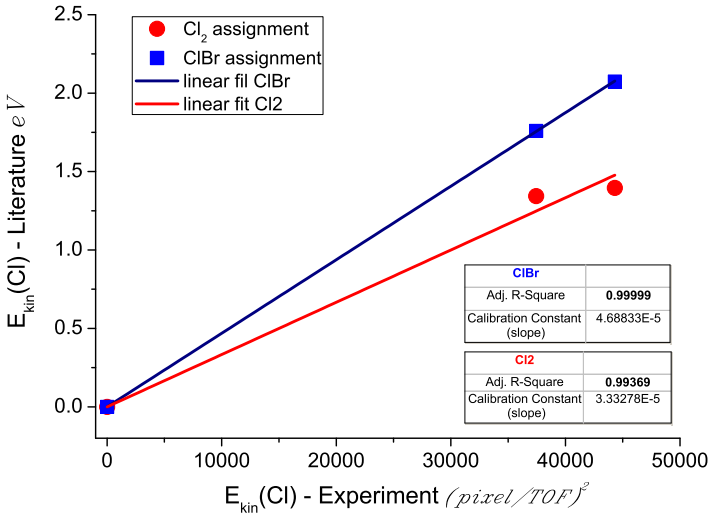

Figure 2.6: Wrong Cl_2 and correct ClBr assignment of observed dissociation products, demonstrated on correlation with expected values.

The linearity of the fit during the calibration procedure is important indicator of the correctness of the assignment of the observed structures to particular processes. Not only the processes, but even the precursor molecules can be assigned incorrect. We can see it on the example on Fig. 2.6. A goal of our study was to explore photodissociation dynamics of the Cl_2 molecule to test our new laser system tunable to Cl REMPI

wavelengths. The assignment to expected energy values for Cl atom dissociating from Cl_2 simply fail to be fitted. The explanation is that Cl_2 interacts with the deposits in the inlet system previously used for HBr. The reaction results into formation of ClBr molecules with much higher absorption cross section at 235 nm in comparison to Cl_2. The correctness of the linear fit for ClBr is demonstrated on Fig. 2.6.

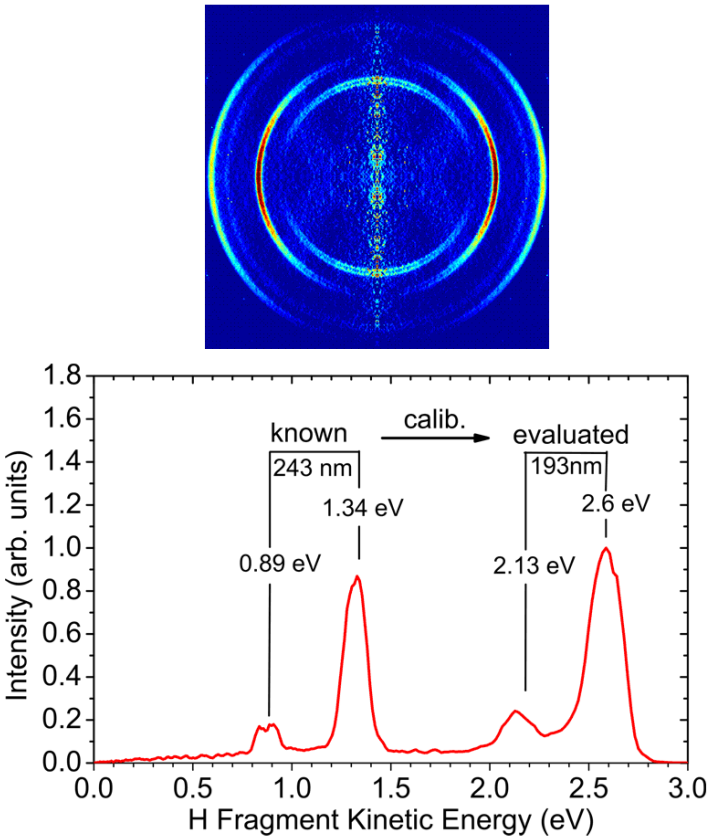

Figure 2.7: Abel transformed velocity map image of H fragment from photodissociation of HBr at 243 nm 193 nm (top). Apropriate H fragment kinetic energy distribution calibrated on known values of 243nm photodissociation demonstrating the process of evaluating the "unknown" values.

The calibration constant is valid for image of same photofragments and at same VMI voltages. For hypothetical diatomic molecule XY the calibration constant A known for fragment X should be multiplied by m_x/m_y for fragment Y. Total kinetic energy released in the process (TKER) can be found from kinetic energy E_x of fragment X according to:

$$TKER = E_x.\frac{m_{xy}}{m_y}$$

Once the axis is calibrated, we can estimate the values of energy for unknown processes from images. To stay with our example HBr molecule we add the ArF laser for photodissociation and assume that we know nothing about the energetics of the observed

features. The sample image is on Fig. 2.7 together with apropriate H fragment kinetic energy release spectra calibrated by constant obtained from dissociation at 243 nm. We can see that two additional features are peaking at 2.13 eV and 2.6 eV. The values obtained are in good agreement with theoretical prediction according to the energy diference between 243nm and 193nm photons (see table 2.4)

2.4.3 Angular Distributions

We already discuss the importance of angular distributions in chapter 1 and we also explore its details for HBr photodisociation in this chapter.

Table 2.5: Evaluated β parameters for hydrogen atom dissociated from HBr at different wavelengths

wavelength	Br state	β present work	fit error bars
243nm	Br	-1.06	-1.15,-0.97
	Br*	1.93	1.4, 2.45
193nm	Br	-0.92	-1.02, -0.86
	Br*	-0.77	-0.98, -0.56

An angular distribution of photofragments for particular dissociation process can be obtained by integration of already back transformed 2D cut of Newton sphere through the velocity distribution of particular transition. The integration procedure once again depends on the analysis software and will not be discussed in detail. The example of the angular distribution spectra for particular transitions of HBr are on Fig. 2.8 together with appropriate integration regions marked on images.

A main output of the angular distribution measurements is the value of β parameter characterizing the transition. β parameter can be obntained by fitting the function according to eq. 1.3 to the angular distribution of photofragments. The values for HBr obtained in our experiment are in Tab. 2.5. In principle eq. 1.8 should be used since the photodissociation and following ionization is multiphoton process. However, a low hydrogen polarizability and its orbital symmetry [7] results into vanishing of alignment effects. Additional Legendre polynomials in the fitting function didn't change the β parameter values, even the spectra for 193 nm seems to have a bit different shape. The effect is more pronounced in the case of atoms with higher polarizabilities or multiatom fragments.

[7] total angular momentum J$\leq$1 see table 2.4 ref[76] case B.

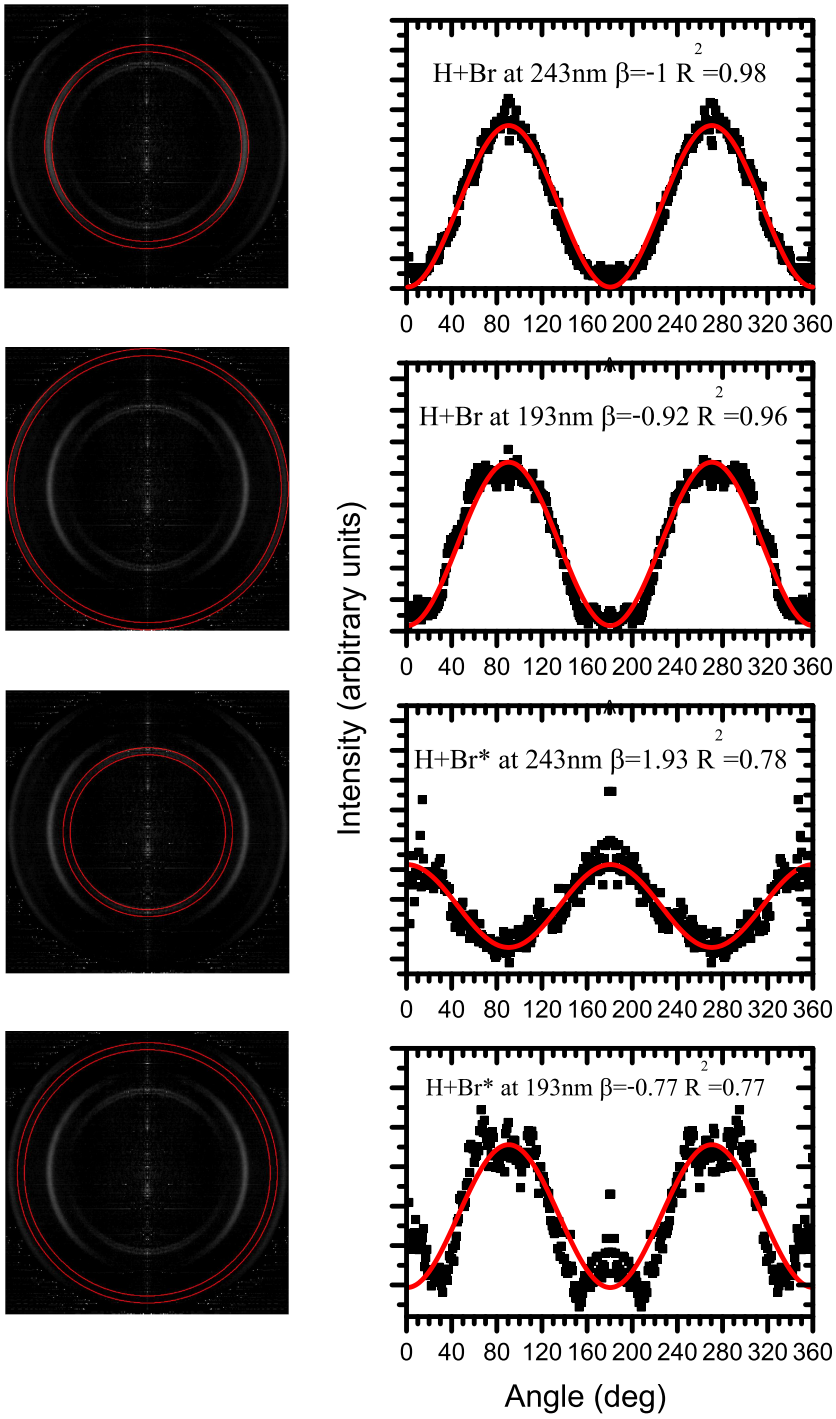

Figure 2.8: Angular distribution of hydrogen photofragments after photodissociation of HBr by 193.3nm and 243 nm photons. Concentric circles on left side images represents the velocity integration region used for particular angular dependence curves on the right side.

We found interesting the question of uncertainty in the determination of β parameter. We can see that fits are not ideal and they often result in low R^2 values (Fig.2.8). The R^2 give us the information about overall fit quality but no information about β uncertainty. For this we have to find the weight of the parameter in the fitting pro-

cess. Easy way is to plot the minimum of the least squares sum dependence on the β parameter value. This way we can see directly how the parameter influences the fit, if it lies in global minimum and also the symmetry of the minimum (see Fig. 2.9). In our particular case we introduce 30 % quantile of the least squares minimum to estimate the β parameter uncertainty. The estimated errors are listed Tab. 2.5 (fit error bars). The analysis of angular distributions was succesively used in experiments with CF_2Cl_2 molecule described in ref. [3] (attachment 2).

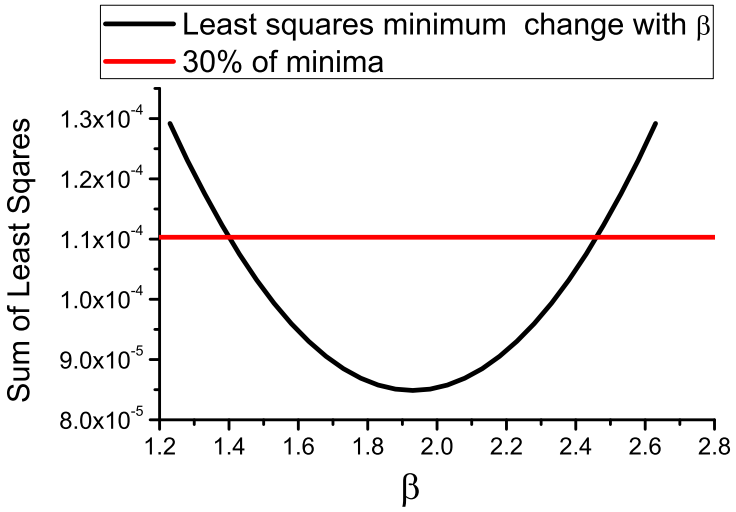

Figure 2.9: To the estimation of β parameter error. The change of least squares minimum value depending on the β parameter includes both the fit quality and beta weight. Therefore, it can be used like simple measure of the fit error of the parameter.

2.4.4 Neutral Beam Temperature

The term temperature is commonly used as a characteristics of molecular beam. However, it is important to say that the main assumption of the molecular beam experiments is that particles do not collide within the beam. Therefore, we should rather speak about the velocity distribution of the molecules in the beam.

Photofragment ion imaging was first used for evaluation of beam properties by Irmia in 2009 [72]. It is based on two simple facts. At first, the image of molecular ions formed after the multiphoton ionization in VMI field represents the distribution of speeds of neutral molecules in the molecular beam. At second, photofragment distribution is shifted with respect to molecular ion distribution due to different flight times [8] what can be used to estimate the neutral beam velocity. Detailed analysis for HBr pulsed molecular beam is in attached article attachment 1.

[8] fragments A and molecular ions AB with zero kinetic energies after ionization will be detected on positions x as $\frac{x_A}{TOF_A} = \frac{x_{AB}}{TOF_{AB}} = v_0$

The article focuses on characterization of pulsed molecular beam expansions of HBr - Rg clusters. First important result of the work is the demonstration of the fact that in pulsed expansions the molecular beam characteristics significantly changes within the pulse. At certain conditions we can have molecules in a one part of the molecular beam pulse and clusters in the other part. This way we can study different chemistry at different delays between photodissociation laser and molecular beam pulse.

Second important result is the demonstration of the fact that clusters formed in HBr coexpansion with rare gases are $HBrRg_n$ with structure of HBr in Rg shell. Photodissociation of HBr in such clusters results into effective caging of dissociation products and strong 0 eV peak in kinetic energy spectra. Both results explain many discrepancies in previous photodissociation dynamics studies with pulsed molecular beams, especially the assignment of central 0 eV kinetic energy peak to dimer, as discussed through the article.

2.5 Slice Imaging

We already mention the advantage of slice imaging - elimination of an image back-transformation. Orientation of the laser beam viewports on CLUB experimental setup is under angle 17° which breaks the symmetry needed for inverse Abel transform. Therefore slice imaging will be of great advantage in experiments on CluB. We try to implement the slice imaging on AIM apparatus in first step. Unfortunately, the time we invest into its implementation was simply not sufficient to reach the optimal performance.

We used the AC slicing approach of Kitsopoulos [62]. In experiment, a cloud of photodissociating fragments expands in the field free region and then it is extracted towards the detector by pulsing the repeller plate. We used Behlke HTS 61 - 03 GSM switch for pulsing the repeller. Expanded photofragment cloud is then cut into slices by pulsing the detector. The pulser was already described in discussion of mass gating in section 2.2. For proper operation grid must be added on extractor plate (to avoid penetration of external field into the region during the cloud expansion). We used Precision Eforming 45 μm grid, which was attached to the extractor plate by small amount of carbon spray. Sample image is on the figure 2.10. We can see distortions of the image. We didn't find the explanation for the distortions but we observed the reduction of the distortions with increase of the ion acceleration voltage. We expect that the distortions can be caused by external fields or by velocity component in the direction of the molecular beam, which can be reduced by shorter flight times. Unfortunately the maximum voltage we achieved in pulsed mode without breakdowns on used HV BNC feedthroughs were U_{ext} =2.34 kV and U_{rep} =2.34 kV + 1.45 kV(pulsed). The delays used were $\Delta t_{laser-repeller}$ = 2.34 μs (140 ns true ion cloud expansion time) and

$\Delta t_{laser-detector} = 3.4\ \mu s$.

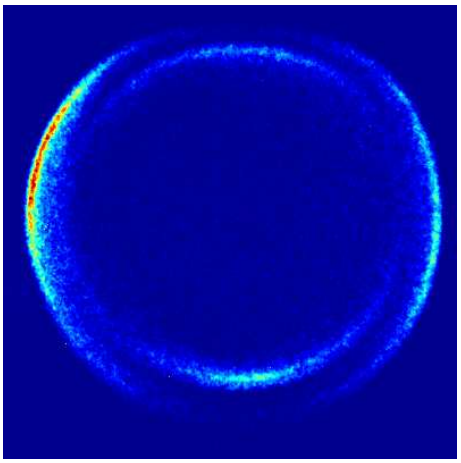

Figure 2.10: Raw data H^+ sliced image from HBr dissociation at 243 nm. We can see the distortion of image and the lower resolution in comparison to abel transformed images (e.g 2.7)

Since the change of the vacuum feedthroughs to more convenient SHV requires significant modification of the setup as well as an investment we did not continue in the developing the slicing in the lab. It can be nice future project on AIM experimental setup. Without changing the feedthroughs it can be possible to make slicing in DC mode (see e.g. [63] or more advanced configuration [108]). However, this will require a modification of the lens system.

3. Experiments on CLUB

The CluB is complex experimental setup developed to study photodissociation dynamics in molecular beams of clusters. CluB is unique due to its ability to study size selected neutral clusters. The size selection will be discussed in part 3.2 together with first results obtained on new VMI implemented within the thesis. Additional technique implemented on CluB within thesis is the high resolution TOF mass spectrometry. Main issues and first measurements will be discussed in part 3.3. Before we explain the measurements we should start with short overview of the experiment.

3.1 Experiment Overview

CluB is a state of the art Molecular Beam (MB) experimental setup developed in the group of U.Buck at Max Planck Institute in Gottingen. Since 2005 the apparatus has been the headstone of our group. In 2011 the system was significantly upgraded. We renew the vacuum pumping system, purchase new light sources (FineAdjustment dye laser and LaserVision IR-OPO) and implement two new methods which are described within the thesis - velocity map imaging and high resolution mass spectrometry. The experiment was explained in detail in several works, most recently in ref. [17].

The CluB was designed as a complex experimental setup employing a compact source of size selected clusters. The cluster size selection based on the elastic collisions with the helium molecular beam is restricted to small masses. Therefore, vacuum system was designed for expansions from low stagnation pressures (bar range) forming only small clusters. The design results in a significant reduction of pumping speeds in comparison to other continuous molecular beam setups $\rightarrow$ compactness. Still it is nearly 3 m high and 4 m long system of high vacuum chambers and pumps and one additional room with a fore vacuum and cooling support. The scheme of the evacuated part of the setup is on Fig. 3.1.

A studied sample is expanded into the vacuum through a simple nozzle or more sophisticated liquid/vapor expansion sources. After the expansion, formed molecular beam pass through a skimmer into the scattering chamber. In scattering chamber, clusters in the beam are deflected by the perpendicular helium beam according to their mass. The next (selector chamber) is housing a pickup cell and two beam chopping wheels. The pickup cell is small region with increased pressure, where the molecules dosed into the cell can stick on the clusters passing through. Alternatively the metal pickup cell is used where solid molecules can be evaporated. One of the chopper wheels is the velocity selector used complementary to the helium scattering in the cluster size selection procedure. Second of the choppers is pseudorandom and it is used for a precise measurement of velocity distributions of molecules in the molecular beam. The

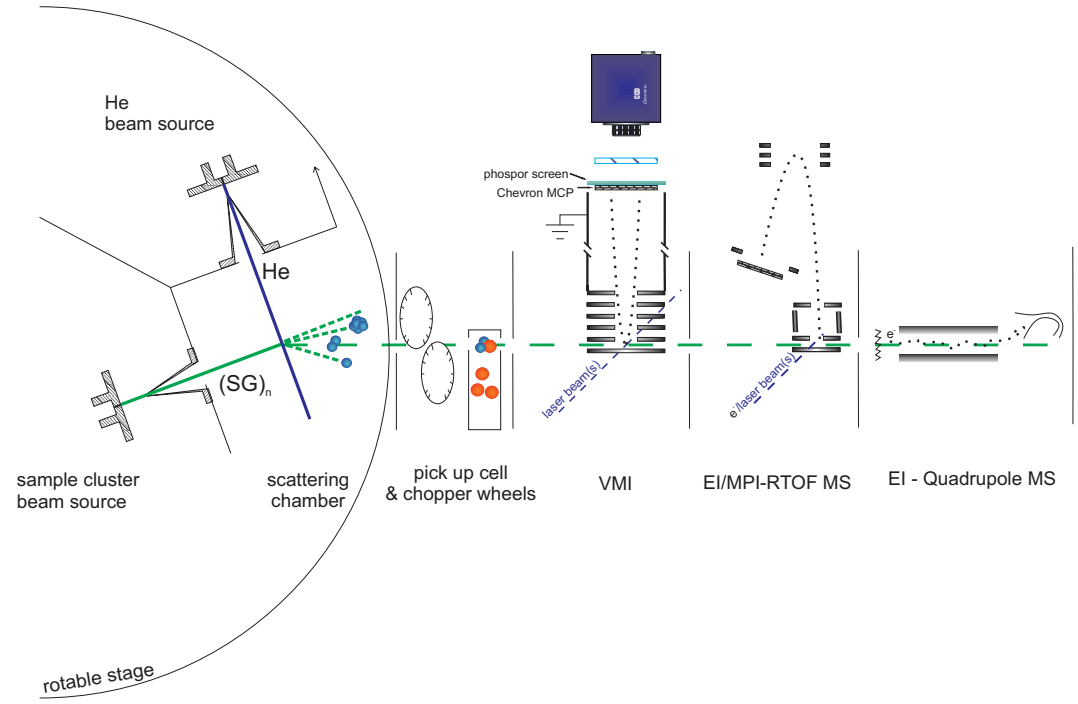

Figure 3.1: Sketch of vacuum part of CLUB experimental setup.

measurement is based on the cross correlation method[109], which will not be discussed in details within the thesis. We use it e.g. during the measurements of adsorption cross sections, described in our work [4]. In the fourth chamber, 60cm from the expansion source there is the first analyzing technique – photofragment ion imaging, which will be discussed in more detail in following text together with new TOF mass spectrometer implemented within thesis.

In the last chamber, there is Extrel quadrupole mass spectrometer able of continuous monitoring of the molecular beam stability. It uses mesh cup cathode with huge electron emission in mA range which results in high sensitivity of the spectrometer. Except the beam alignment it is used also in the velocity distribution measurements in the combination with pseudorandom chopper.

3.2 Photodissociation Dynamics of Size Selected Clusters

The study of photodissociation dynamics of size selected clusters was an ultimate goal of the dissertation. The idea of the experiment is depicted on Fig. 3.2. In first step a beam of clusters is formed, which is crossed by perpendicular beam of helium atoms. The clusters are deflected into different angles according to their mass, what is simple result of momentum conservation. By rotation of the beam source in respect to the rest of the experimental setup, we can study clusters in size range under the

theoretical mass value for specific angle. What is more important this way also the velocities of clusters are differentiated according to mass, therefore full mass selection can be achieved incorporating the velocity selector in the next vacuum chamber. The size selected clusters are then photodissociated by light from one of the available sources and the products are analyzed by photofragment ion imaging.

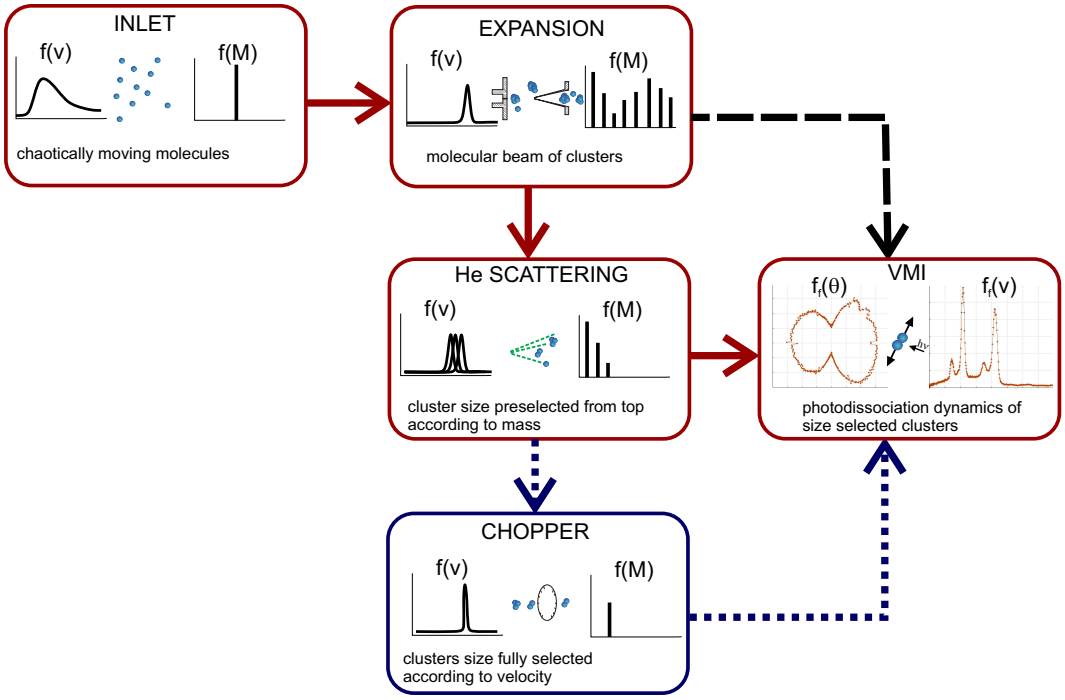

Figure 3.2: Scheme of proposed experiments with size selected neutral clusters. The distributions of velocity f(v) and mass f(M) of particles is sketched for each particular step. In final step photodissociation dynamics of size selected clusters is studied by VMI obtaining velocity and angular distributions of photodissociation fragments $f_f(\theta)$ and $f_f(v)$ respectively. The part of the scheme followed in recent experiments is marked by red arrows. Alternative of full size selection and no size selection are marked by dot and dash arrows respectively

The progress of this part of the dissertation was significantly influenced by the lack of suitable laser source. The concentrations of precursor clusters after size selection are extremely low and even resonance enhanced detection scheme for hydrogen is still 3 photon process requiring significant laser intensities. The intensities were expected to be achieved by new laser system purchased in 2011. However, till nowadays the system is not reaching the parameters of the old dye laser system in our lab (nearly 20 years old!). First results achieved at low laser powers are discussed in following text.

3.2.1 Size Selection

The neutral cluster size selection by helium scattering was developed in the group of U. Buck [110] and to our knowledge it is unique for our experiment. So far there is no other experimental technique beating this simple mechanistic approach. The

experimental techniques used for neutral size selection are usually restricted to larger systems (aerodynamic separator typical for atmospheric aerosol studies was applied e.g. in the work of Piseri [111]).

A promising approaches to size select small neutral clusters come out of a quantum world of matter wave optics. First experiments were performed by Schöllkopf and Toennies using transmission gratings [112]. Except transmission also the reflection gratings were used so far [113, 114]. However, the sufficient resolution can be achieved only at long distances from the cluster source. At such a long distance concentrations in the beam are at detection limits of current experiments. The most promising technique so far is that of Marcus Arndt incorporating the Talbot Lau interferometer [115, 116]. In the technique a light grid is used at wavelength 157 nm, enough to ionize the beam constituents. This way the grid made of ions is formed which are reflected in following step and only size selected molecules are detected. The problem of usage of the technique together with clusters is in the dependence of the interference pattern on the polarizability of molecule. This value could vary for clusters therefore the usage is somehow questionable.

Another approach to size dependent measurements of neutral clusters is qualitative. In qualitative approach, techniques are not focused on the cluster size selection but rather on the characterization of the size distribution in the beam. In the case of molecular beams the size distribution can be changed by varying the expansion conditions. The knowledge of the distribution can be then used to make conclusions about the process dependence on the cluster size. The most commonly used techniques are sodium doping [5], poisson distribution after pickup [117], momentum transfer after pickup [4], cluster deposition on the surfaces [118] or NMR spectroscopy[119].

Qualitative approach was used in several HBr cluster experiments, discussed in the part 2.4. One of the conclusions is that caging effect is more effective with increase in the cluster size. However, it is clear that even the caging effect is not monotone function of the cluster size but rather depends on the number of layers around the dissociating molecule. Similar, according to calculations [25] already one molecule can have significant effect on photodissociation dynamics and it is important to see how these effects are evolving step by step. For such experiments qualitative experiments are insufficient, since distribution of variety of cluster sizes is always present in unperturbed molecular beam.

In recent experiments we did not succeed to use full size selection scheme. However, even partial cluster size selection experiments reveal interesting behavior like discussed in following chapter. Before we unveil the photodissociation dynamics results, lets have detail look on the used size selection via He scattering.

The method is well described in chapter 3.3 page 31 of ref. [17], we will focus on particular results obtained for $(HBr)_n$ clusters. The selection is based on perpendicular collisions of He atoms with particles in the molecular beam. To achieve reasonable

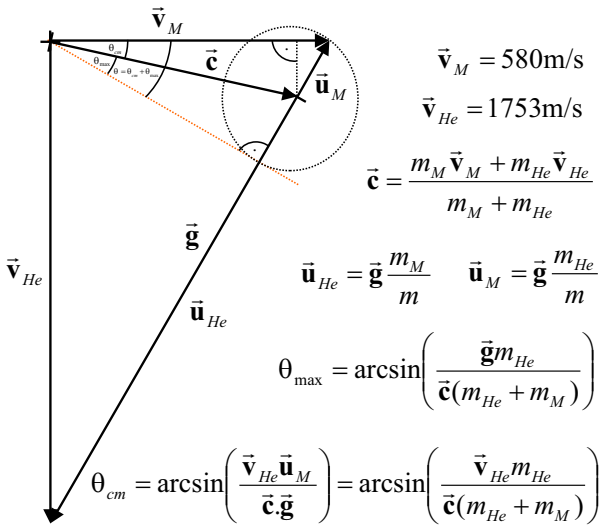

Figure 3.3: To the calculation of maximum scattering angle θ in laboratory frame. The results for $(HBr)_n$ clusters are summarized in table

Table 3.1: Calculated scattering variables for first 8 $(HBr)_n$ clusters

cluster	$\vec{c}$	θ_{max} [°]	θ_{cm} [°]	θ [°]
monomer	558.8	8.95	8.49	17.4
dimer	567.6	4.5	4.27	8.8
trimer	571.3	3	2.85	5.85
tetramer	573.3	2.25	2.14	4.4
pentamer	574.6	1.8	1.7	3.51
hexamer	575.4	1.5	1.42	2.9
heptamer	576.1	1.28	1.22	2.5
octamer	576.5	1.13	1.1	2.2
nonamer	576.9	1	0.95	1.95

results, single collision conditions must be fulfilled. The collision parameters as well as the computed scattering angles for selected HBr clusters are in the tab. 3.1. We can see that reasonable differences between threshold scattering angles are only for small clusters up to $(HBr)_6$. These provides intervals to study monomers ($8.8° - 17.4°$); monomers and dimers ($5.85° - 8.8°$); monomers, dimers and trimers ($4.4° - 5.85°$)... Angular dependence of the measured signal for monomer and dimer ions is on fig. 3.4. We can see that dimer signal really vanish at expected angle of ∼8.8°. Also we can see low intensities of the scattered signal in comparison to primary beam, as well as the low angular spread of unperturbed molecular beam with angular spread under ∼1°.

To fully select the cluster size we must employ the velocity selector in next chamber. We did not do that due to extremely low intensities in present study. Therefore only difference between small and large HBr_n clusters will be explored. The measurements were performed at angle 2.9°. Neutral clusters present in the beam should range from monomer to hexamer. A change in neutral cluster distribution can be seen on the mass spectra depicted on fig. 3.5. In next section, we will explore the photodissociation

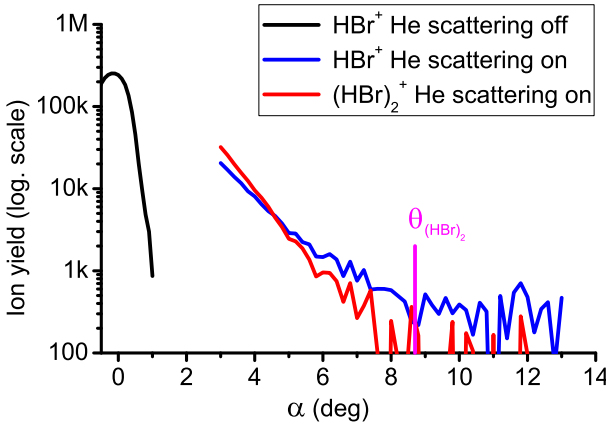

Figure 3.4: Angular dependence of HBr^+ and $(HBr)_2^+$ signal after He scattering. Figure demonstrates the correctness of the scattering method as well as the drawbacks - low intensity of the scattered signal and a low resolution of the method incorporating only He scattering.

dynamics of $(HBr)_n$ clusters in these two cluster size ranges.

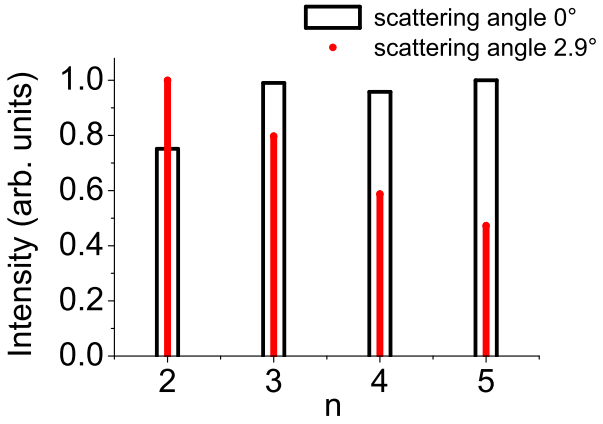

Figure 3.5: Mass spectra of HBr clusters after He scattering. In primary beam spectra is peaking at pentamer ion reflecting the fragmentation of large clusters. At deflection angle of 2.9° signal is peaking at monomer ion with rapid decrease to higher masses reflecting the fragmentation of small clusters.

3.2.2 Velocity Map Imaging

A VMI implementation on CluB was expected to proceed in 2 steps – built of a test VMI setup on independent vacuum system and its move to CLUB apparatus. The progress of the first part was described in chapter 2 - Experiments on AIM. However, we realized that AIM system can be used independently and new VMI detector was designed for the CLUB apparatus. The VMI stack copies the design on AIM. We used different detector and power supplies. Complete detector was purchased from TOPAG and consist of chevron MCP plates of 50/41 mm outer/active diameter and P43 phosphor screen. MCPs are connected through 5kV SHV and phosphor through 10 kV SHV

connectors. MCP electronic signal is measured on 1kΩ resistor coupled to HV through 2x222 ceramic capacitors connected in series (total capacity 1100 pF). No resistors were added to MCPs, since they are well matched and also the safe current through MCPs can be controlled by used power supply. Power supply is custom built Iseg THQ unit with 2x5 kV + 1x6 kV DPS modules. The goal of the improvement was to secure the operation in the ion counting mode. The ion counting mode requires high and stable voltages on both MCPs and phosphor screen. Recently we implement a new camera with acquisition software developed in A. Suits group [120] allowing the centroiding and further improvement of signal to noise ratio. However the data presented within the chapter were still obtained using same Unibrain camera and acquisition software, as used on AIM apparatus.

Main problem of the VMI implementation on CLUB is the fact that the molecular beam can not be moved. On test measurements, we have seen that VMI is highly sensitive to the position of molecular - laser beams cross point. The significant improvement will be the tilting of VMI stack from outside the vacuum system. The improvement will require modification of the vacuum chamber holding the VMI, that we try to avoid during thesis. Now the tilting of VMI can be done only inside the chamber - after breaking the vacuum. Vacuum turn offs significantly slow down the tuning procedure. The procedure is same like on AIM , therefore we are not going through it once again.

The only results we obtained on new VMI are for HBr clusters. Velocity map images for two different He scattering angles (cluster sizes) are on Fig. 3.6. Image at position 1a), b) of Fig. 3.6 shows the hydrogen photofragment velocity map after photodissociation of HBr in large clusters. Expansion conditions were set to produce the cluster distribution with mean size of tenths of molecules (∼40 for pure Ar beam). We can see the molecule features known from the images discussed in chapter 2. Additional feature occurs in the middle of the image as the sharp peak of zero kinetic energy fragments. These are hydrogen fragments produced by dissociation of HBr inside the cluster and slowed by follow up collisions with neighboring molecules. High speed of the hydrogen fragment after photodissociation dictates classical character of the collision process [1] . Of course such collisions can result into excitation of the molecules within cluster. Concerning speed of photofragments (∼15000m/s) and dimmensions of cluster (nm) it is clear that collisions can occur on time scales shorter than laser pulse length (ns). Excited HBr are therefore dissociated within the same laser pulse. Such photodissociation results in additional ring of hydrogen photofragments in outer part of the image.

The image on position 2a) b) of Fig. 3.6 shows the hydrogen photofragment velocity map after the photodissociation of HBr in small clusters. Small clusters were prepared by He scattering method described in previous section. At studied deflection angle we

[1] DeBroglie wavelength of the hydrogen photofragments is ∼0.26 $\AA$

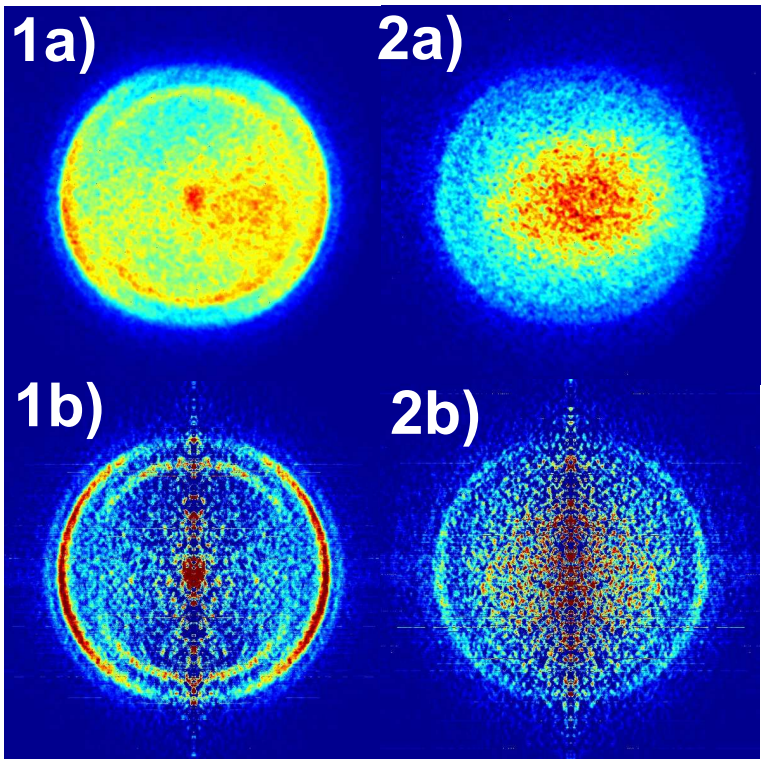

Figure 3.6: Velocity map images of hydrogen photodissociating from neutral HBr clusters of different sizes. 1 - Large clusters with probnounced caging as well as vibrational excitation effects 2-clusters up to tetramer with nearly no caging but still observable intensities of vibrationally excited fragments. a) and b) represents raw data and apropriate Abel transformed images

can study the clusters up to maximum size of hexamer. We can see that central feature vanish at this angle what further supports our explanation of the zero kinetic energy photofragment signal. Simply small clusters up to pentamer lack the cage structure. On the other hand, there is an increase of diffuse signal in the central part of the image from zero eV to dissociation limits. It is well demonstrated on comparison of KEDs on Fig. **??**. The increase can be still caused by H fragment collisions with neighbouring molecules within the cluster. However, the number of collisions in the small system is not enough to fully stop the fragment. The conclusion is further supported by observation of outer ring from vibrationaly excited fragments. We were not able to employ the full size selection or to perform the measurements at larger angles (smaller clusters) to find the threshold for vibrational excitation within the clusters. It is caused by insufficient laser intensities to perform these low signal measurements. E.g. the acquisition of image on fig. 2a) takes 10h what makes high demands on the stability of molecular beam as well as the experiment expenses.

Recently, we are working on implementation of the centroiding approach to data acquisition which will improve our signal to noise ratio in ion counting mode. In combination with improved laser intensities we believe in successful continuation of the experiments in near future.

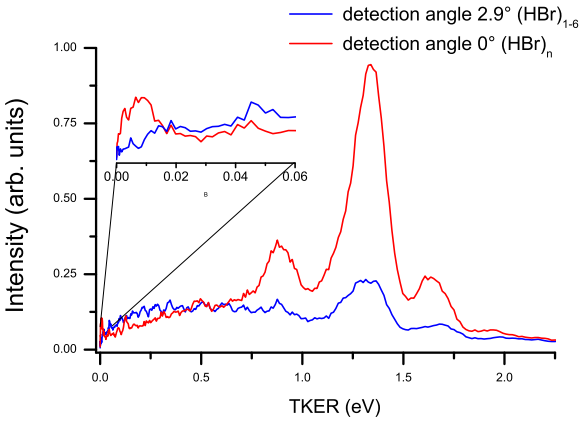

Figure 3.7: Kinetic energy distributions obtained by radial integration of images on fig. 3.6

3.3 Implementation of Time of Flight Mass Spectrometer

Within the thesis a new mass spectrometer was implemented on CluB experimental setup. The idea was to purchase TOF mass spectrometer with improved resolution and mass range in comparison to our old Extrel quadrupole. On the other hand we want to keep the quadrupole for cross correlation measurements, that requires the use of TOF in configuration perpendicular to the molecular beam axis. Next requirement was ionization source, since we want to use both electrons and any of our laser sources to induce ionization. Finally, special requirement was on the sensitivity of the instrument, because of extremely low concentrations of molecules in molecular beam 1.3m from the nozzle (at planned TOF position). Lets have a look on how particular requirements influence the selection procedure.

The main complication of the TOF implementation is the orientation of spectrometer perpendicular to the molecular beam axis. It is problematic due to huge differences in kinetic energies of single particles in the direction of molecular beam.

The main advantage of a molecular beam approach is a transformation of thermal and internal energy of particles into motion in the direction of the molecular beam. This way all the particles in the beam are moving in the direction of the molecular beam with speeds ranging from hundreds to thousands of meters per second and velocity spread in percents of the beam speed (see chap 1 and publication [1] for more details). On the other hand, we have huge distribution of masses in the molecular beam ranging from single molecules up to clusters of several hundreds of molecules. The result of the nearly same speed in the direction of the molecular beam and wide mass distribution is huge energy spread of particles in the direction of the molecular beam. Such energy spread results in dispersion of particles after extraction perpendiculary to the molecular beam axis.

By the way of example Ar monomer and Ar_{100} cluster in the beam with same speeds of 500 m/s will have kinetic energies in the direction of the molecular beam 52 meV and 5.2 eV, respectively. Extracting the same particles after ionization by 1 kV/cm extraction field [2] perpendicular to the molecular beam we get 1 m flight times of 20.3 μs and 203 μs [3] and ion distance in the direction of molecular beam of ~10 cm. Therefore at least 10 *cm* detector will be needed to detect all the ions. Since the price of such detector will exceed the half of the price of the whole instrument we were forced to find different solution.

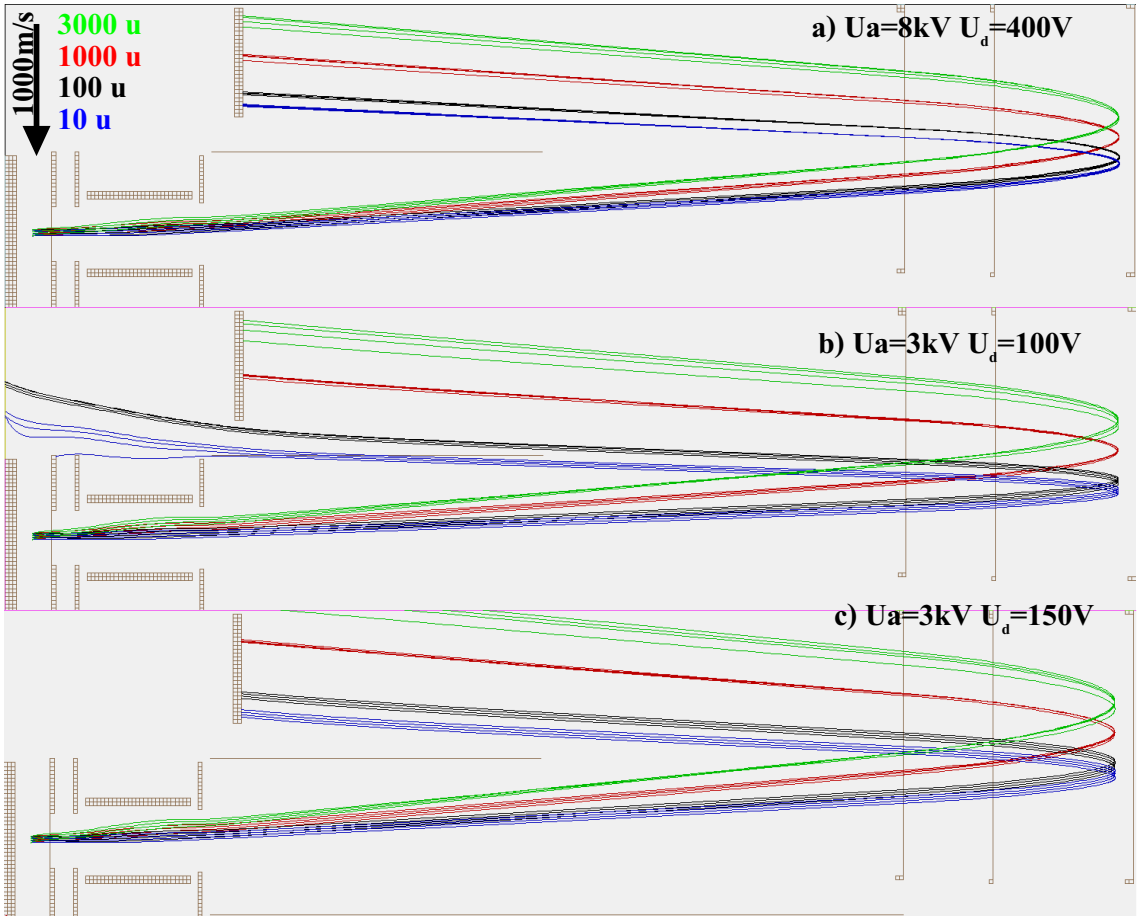

Figure 3.8: Simplified sketch of reflectron TOF showing the effect of acceleration voltage U_a and deflection voltage U_d on detection efficiency. In high field all the ions in 10u - 3000u are detected. In lower field mode only part of the spectra can be obtained depending on the deflection voltage settings.

There were three solutions offered by companies. The most simple and often used solution is an addition of deflection plates into the post extraction region of spectrometer. We can see on Fig. 3.8 that the deflection does not solve the problem. By changing the deflection voltages we change the position of ions on the detector, however we do not

[2] $500V$ in the middle of the extraction region typical for commercial TOF mass spectrometers available in our price range

[3] $t = \frac{l}{\sqrt{2U}} \cdot \sqrt{\frac{m}{z}}$

influence their spread and therefore at specific deflection only part of the mass spectra can be detected. A collection of whole mass spectra will require several measurements at different deflection voltages.

Another proposed solution was the ionization in the direction of the molecular beam and ion deflection using quadrupole deflector. Once again it does not solve the problem due to simple phase space conservation. Once we set the deflector in manner to focus the energy spread we result in spatial distribution of fragments which can not be furhter processed without significant loss in intensity.

The same holds for the third system proposed, which employs the deceleration field after ionization, still in the direction of the molecular beam followed by the extraction of slowed ions. Additional disadvantage of the last two mentioned approaches is the long time between ionization event and ion extraction into the detector. During the transport ions are accelerated/slowed in the direction of the neutral molecular beam what can result in further reactions between formed ions and neutral beam constituents. On the other hand, both solutions can be used with effective electron ionizers similar to one used on our Extrel quadrupole. However the higher sensitivity does not compensate the problems connected with multiple measurements per mass spectra and influence of mass spectra by ion molecular reactions after ionization. Therefore we try to find alternative solution.

We can see on Fig. 3.8 that easiest way to reduce the spread is the reduction of flight time. The flight time reduction can be achieved by reduction of TOF length or by increase of ion acceleration voltage. To keep the reasonable resolution of the mass spectrometer, only the second option is acceptable. The increase in acceleration voltage is not trivial request since the extraction voltages have to be pulsed (electron ionization option). The only company, which take up the gauntlet was small TOF producer Stefan Kaesdorf from Munchen.

The most interesting characteristics of the realized design are for electron ionization mode. Molecular beam is passing directly through the exraction region of mass spectrometer. Molecular beam is crossed by magnetically colimated beam of electrons. Energy of the electron beam can be varied in 5 eV - 90 eV range. Produced ions are accelerated by 10 kV pulses (5 kV in the center of extraction region). Electron gun is also pulsed and the delay between the electron gun pulse and extraction pulse can be varied, to avoid the reactions of accelerated electrons with neutral molecules during the ion extraction pulse. Extracted ions are accelerated to 8 kV to fulfill the Wiley Mcleren condition in present ion optics configuration. Ions passing the reflection mirror are then detected on 4 cm MCP detector. Except the significant reduction of the ion dispersion, high acceleration voltage solves another problem of cluster ion mass spectrometry. The low sensitivity of MCPs to high masses. The problem is exactly the inverse of problems with energy spread in the direction of molecular beam. Kinetic part of secondary electron emission coefficient is according to Parilis Kishinevski theory

dependent on the speed of impact particles. Since the energy of the clusters obtained in the accelerating electric field is same the velocities of large particles are lower and apropriate gama coefficient is also much lower for heavier particles. (for details see e.g. [121]). The low effectivity of MCPs in high mass ion conversion is usually solved by acceleration grid in front of detector. In our system the impact energy of ions is 8 keV which is enough to reach reasonable efficiency in studied range up to 5 kDa.

There are several other advantages of the purchased TOF spectrometer. At first data acquisition proceeds via TDC method. It significantly reduces the amount of processed data and high resolution TOF data with time step as low as 0.25 ns can be recorded. Such high resolution data can be used for data mining from TOF peak shapes, e.g. for ion decay studies [122, 123]. Of course it is possible to measure with longer time steps and such measurements results into significant improvement of intensity (the intensity is always sum of intensities in base 0.25 ns bins). Second advantage is high repetition frequency of the spectrometer up to 12kHz. It means that dynamic range of measured spectra 10^7 for low intensity measurements in cluster studies can be achieved within minutes,[4] beating the performance of most of the commercial mass spectrometers.[5] Aditional advantages are e.g. in configuration of acceleration voltages in Willey McLeren condition further improving the resolution or mass gate which allows to deflect selected fragments (e.g. intense monomer signal saturating the detector during cluster measurements).

The mass spectrometer was used in standard mass acquisition mode in our first study on HNO_3/H_2O mixed clusters [5]. Changeability of electron energy of the ionization source was fully employed in our study of acetylene clusters attached [6] (attachment 5). Short flight times in our experiment allow us to study also the metastable decay of cluster ions. Preliminary results are presented in following chapter "Energy dependent fragmentation of water clusters" to give the reader idea about the measurement and future plans.

3.3.1 Energy Dependent Fragmentation of Water Clusters

Relatively long lifetimes of cluster ions allow the parent/daughter ion distinction in two stage reflectron TOF spectrometers. The measurement is based on fact that signal

[4]Maximum intensity in single spectra obtained by TDC method is 1 and to reach 10^7 range we need to measure 10^7 mass spectra. At repetition frequency 12 kHz it can be measured within 14 minutes

[5]There are TOF mass spectrometers reported with repetition frequency up to 200 kHz [124], but the number is quite disputable. E.g. in cited work the extraction pulse length reported was 4 μs leaving only 1 μs for time of flight at 200 kHz. At TOF length 1 m and expected acceleration voltage ~1 kV we end up with maximum detectable mass of 0.2 Da. For reported 1 kDa mass spectra we end up with flight time 72 μs which gives together with 4 mus extraction pulse maximum operating frequency of spectrometer ~13.2 kHz. At comparable frequency of 12 kHz we are able to detect spectra up to ~10 kDa due to higher acceleration voltage 8 kV and shorter extraction pulses 1 μs

of ions formed by parent ion dissociation in first stage of reflectron is shifted in respect to parent ions penetrating into second stage. The shift results into peak splitting like described in works of Castleman group [125, 126]. The effect was observed in our current study of water clusters. We try to combine the observation with energy dependent measurements to reveal the energy dependent fragmentation probability of the clusters. Parent and daughter ion signals were disentangled like it is depicted on Fig. 3.9.

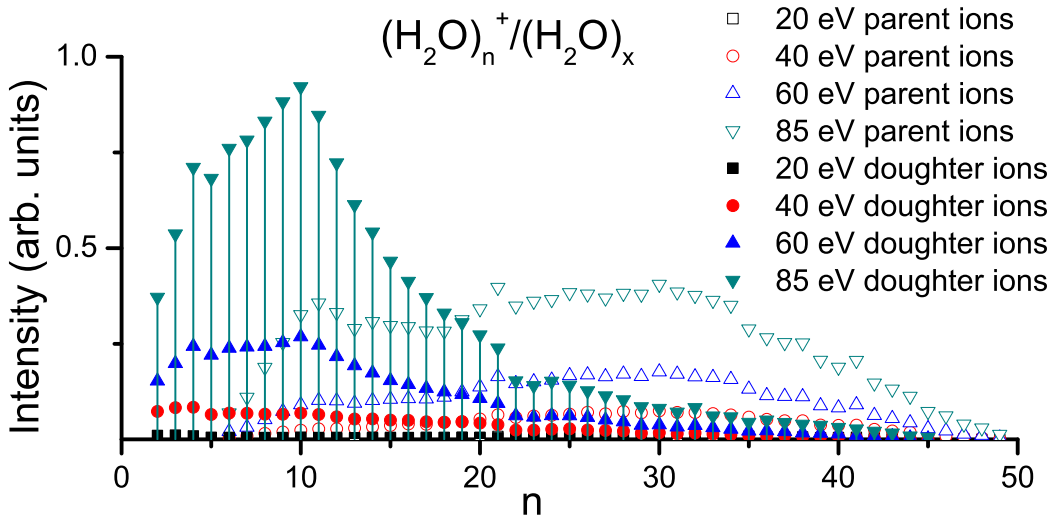

Figure 3.9: Parent and daughter mass spectra of $(H_2O)_n^+$ ions formed in electron ionization of $(H_2O)_x$ clusters at diferent electron energies.

In next step the intensities were summed and parent to total ion signal ratio was obtained at different energies. We can see from Fig. 3.10 that the ratio is decreasing with the electron energy. Simply, higher impact electron energy results into higher energy available in the system and higher fragmentation of ions. Interesting information is then obtained by extrapolation of the signal to the ionization limit observed for studied water clusters ~12 eV. We end up with the ratio of ~0.6, which indicates that even by ionization at threshold we will have significant amount of ions fragmented. It is caused by the exothermic character of the water cluster ionization at threshold due to high stability of water dimer ion as well as by the detection time in our experiment. To disentangle the two contributions time dependent measurements will be needed. The detection time can be varied by acceleration voltage variation or ionization/extraction delay variation. The measurement presented here performed for different detection times can give us the information about lifetimes of ions. In final step contribution to decay due to impact electron energy can be clearly identified. Presented data are therefore only preliminary demonstration of the important mass spectrometer feature, which will be used in forthcoming studies.

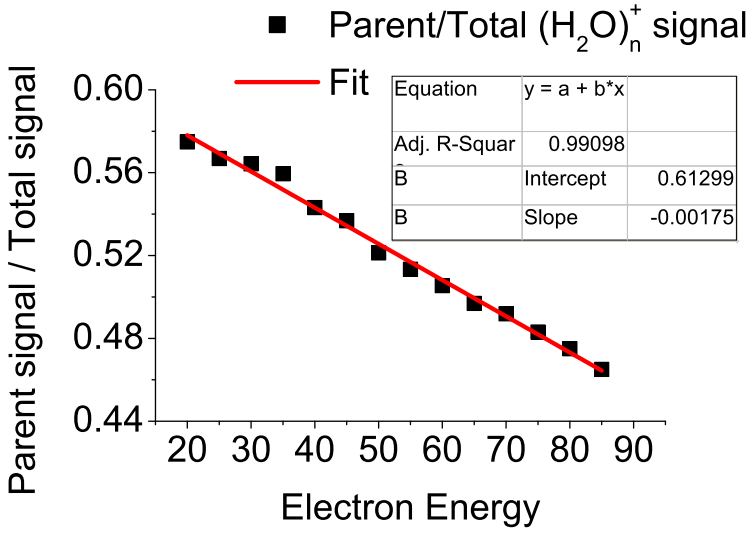

Figure 3.10: Dependence of cluster fragmentation on the energy of impact electron.

4. Acetylene Chemistry in Clusters

All my work during the thesis was glued by the theme of acetylene clusters. We studied electron and photon induced reactions in acetylene clusters to reveal details of an environment influence on the reactions. Such studies are crucial for understanding of the formation of complex molecules from simple precursors like acetylene, its ions or its photodissociation products. The research is described in three attached publications.

Acetylene is important technical gas with applications ranging from welding to polymer industry. Similar its importance in nature can not be completely described on one place. Acetylene is most simple hydrocarbon containing triple bond evoking high interest for fundamental reasons. The triple bond stores large amount of energy, which can be used to overpass barriers of complex reactions. Therefore acetylene is extensively studied in connection to formation of complex molecules. Such formation is crucial to understand fundamental processes in space, atmospheres, during combustion or in acetylene containing plasma. We focus on environmental effects on the electron and photon induced reaction of acetylene. These were studied in clusters. Electron and photon reactions leads to the formation of reactive precursor radicals and ions, which can effectively interact with other cluster constituents.

The first publication "Short review on the acetylene photochemistry in clusters: photofragment caging and reactivity" summarizes previous studies of acetylene photochemistry in clusters carried out in our group. Previous results are supported by the results obtained on AIM experimental setup within thesis. We achieve the molecular regime in pulsed expansion what was not possible in previous experiments with continuous molecular beam. Most important result is the observation of quantum mechanical caging effect partially described in introduction. Work also opened questions of alternative explanation through formation of more complex molecules, which were observed in acetylene clusters previously. In context of complex molecule formation is interesting parallel publication published in WDS proceedings.

The second (WDS) publication "UV Photodissociation of Acetylene in Various Environments" reveals a periodic structures in kinetic energy distribution spectra of acetylene clusters. Structures have extremely low spacing in range of hundreds of $cm^{-}1$. There are several possible interpretations from vibrations of soft acetylene - acetylene bonds within cluster up to multiphoton ionization of acetylene followed by quenching into vibrational states of similar geometry followed by dissociation. Unfortunately we didn't find unambiguous assignment.

The third publication is mass spectrometric study conducted by means of time of flight mass spectrometer implemented on CLUB experimental setup:[6]; "Ionization of

large homogeneous and heterogeneous clusters generated in acetylene-Ar expansions: Cluster ion polymerization". The study focuses on differences in cluster structures prepared in different coexpansions of acetylene with rare gas into vacuum. We show that different expansions results into significantly different cluster structures with different amount of internal energy available for intracluster reactions. The interpretations are supported by measurements of appearance potentials using variable energy electron source. The results involve confirmation of the cluster structure of acetylene caged inside Ar or an experimental proof that benzene cation is not the only $C_6H_6^+$ structure formed after electron irradiation of acetylene clusters. These, as well as other details of the work are crucial for understanding the discrepancies in previous works focused on formation of complex molecular ions in process called cluster ion polymerization.

In summary the three works reveal the structure of neutral clusters formed in various coexpansions with rare gases. The interpretations of both photon and electron induced experiments coincide well in interpretation of neutral cluster structure at similar expansion conditions. Photon induced studies show that after irradiation of acetylene clusters by 193 nm light formation of excited acetylene is more probable than the dissociation itself. Such behavior results into significant enhancement of multiphoton processes in comparison to gas phase. Periodic structures observed in the KED spectra of hydrogen opened questions about the structure and reactivity of acetylene excited states. The structures can be the fingerprint of more complex molecules. Electron induced experiments then undoubtedly show the formation of complex covalently bound molecular ions within acetylene clusters.

Table 4.1: Selected properties of Acetylene [127], [92], [128]

Physical	mass	26.01565 (100)
		27.01901 (2.2)
		26.037 (avg)
	boiling point	189 K
	vapor pressure	4.5 MPa at 290 K
Energetics	Enthalpy of formation	-226.73 kJ/mol
	Bond Strength	5.712eV (551.2 kJ/mol) C-H
	Ionization energy	11.4 eV
Structural	Bond Length	1.216A C=C
		1.074A C-H
Other	Autoignition temperature	578 K - 5 98K
	Odor threshold	565 ppm (garlic like)
	Flammable concentrations in air	2.5 % - 80 %

Conclusion

The work maps the progress in implementation of novel techniques to study clusters in molecular beams. Two analysis techniques were implemented - velocity map imaging[1],[3],[2] and time of flight mass spectrometer with variable energy electron ionization source [5],[6].

The complexity of main continuous molecular beam setup in group - CluB does not allow direct implementation and testing of VMI technique. Therefore smaller pulsed molecular beam test apparatus was built - AIM. AIM apparatus was succesively tested on HBr molecule and cluster systems. Test measurements are described in detail to introduce reader into the technique as well as measurement and data interpretation procedures. The work progress by implementation of newly designed VMI system on main cluster beam apparatus CluB. Short introduction into photofragment ion imaging of neutral size selected clusters is followed by first results obtained using this unique combination of experimental techniques. Main issues concerning the implementation of new time of flight spectrometer are also described. Its abilities are then demonstrated in attached publications as well as short section describing recent experiments on metastable decay of water clusters.

Research results of the thesis are well documented in attached and referred publications linked to the thesis. We focused on exploration of solvent effects on chemistry at nanoscales.

Photodissociation experiments with halogenated compunds show strong caging effect in molecular clusters as well as clusters solvated in rare gas. Study of HBr [1] additionally demonstrates the change of expansion conditions within pulse in pulsed molecular beam expansions and its huge influence on observed photochemistry. The first velocity map imaging sudy of CF_2Cl_2 [3] additionally opens the question of dissociative channels involved in photochemistry of gas phase molecule. Previous assignments were corrected on the basis of careful angular distribution analysis and laser intensity measurements.

Photodissociation experiments with size selected clusters of HBr show that caging effect is significantly reduced in case of small clusters (up to hexamer). The cage of several molecules is simply not enough to slow down the outgoing hydrogen photofragment in collision with neighboring molecules. On the other hand the cluster constituents could be effectively excited by collisions even in the case of small clusters. Fast collisional excitation results into observation of photofragments from dissociation of excited molecules within the same laser pulse. The effects of environment on dissociation of hydrogen bromide can be explained on the basis of classical collisions. The situation is different in the case of acetylene clusters.

Our VMI study of acetylene clusters [2] well reproduces the previous TOF stud-

ies and confirms the formation of fast hydrogen photofragments. Their formation is described through quenching of photoexcited state into highly vibrationally excited states of neutral precursor due quantum mechanical cage formed by neighboring solvent molecules. Such cage can significantly influence the shape of dissociative electronic states and increase the probabilities of nonadiabatic transitions.

In conclusion, by dissociation of simple diatomics in solvent, most of the energy is released by interaction with solvent. On the other hand, in case of polyatomic molecules the co-fragment can absorb significant amount of energy into its internal degrees of freedom resulting into two step process. Effective interaction with dissociation co-fragment inside the "quantum mechanical" cage in the first step and energy transfer from excited system into the solvent in second step. Increase in nonadiabatic transition probability into the excited neutral state within the solvent and subsequent photodissociation can be understand like "delayed" multiphoton process. Therefore, solvent environment significantly increases the multiphoton probability. Single photon as well as multiphoton processes leads into effective formation of ethyl radical within clusters. Its further interactions with cluster constituents can result into effective formation of complex covalently bound molecules.

The formation of complex covalently bound ions was observed in study of different - electron induced processes in acetylene clusters [6]. Ions as large as $C_{14}H_{14}$ were undoubtedly assigned to covalent structures formed after electron irradiation of acetylene clusters. Careful energy dependent experiments then correct the discrepancies in previous works concerning the cluster ion polymerization process.

Bibliography

[1] J. Fedor, J. Kočišek, V. Poterya, O. Votava, A. Pysanenko, M. L. Lipciuc, T. N. Kitsopoulos, M. Fárník, Velocity map imaging of hbr photodissociation in large rare gas clusters, The Journal of Chemical Physics 134 (15) (2011) 154303.

[2] M. Fárník, V. Poterya, J. Kočiaek, J. Fedor, P. Slavíček, Short review on the acetylene photochemistry in clusters: photofragment caging and reactivity, Molecular Physics 110 (21-22) (2012) 2817–2828.

[3] V. Poterya, J. Kočišek, A. Pysanenko, M. Fárník, Caging of Cl atom from photodissociation of CF2Cl2 in clusters, Physical Chemistry Chemical Physics (2013), accepted for publication.

[4] J. Lengyel, J. Kocisek, V. Poterya, A. Pysanenko, P. Svrckova, M. Farnik, D. Zaouris, J. Fedor, Uptake of atmospheric molecules by ice nanoparticles: Pickup cross sections, J. Chem. Phys. 137 (3) (2012) 034304.

[5] J. Lengyel, A. Pysanenko, J. Kocisek, V. Poterya, C. Pradzynski, T. Zeuch, P. Slavicek, M. Farnik, Nucleation of mixed nitric acid?water ice nanoparticles in molecular beams that starts with a hno3 molecule, J. Phys. Chem. Lett. 3 (21) (2012) 3096–3101.

[6] J. KoCisek, J. Lengyel, M. Farnik, Ionization of large homogeneous and heterogeneous clusters generated in acetylene–ar expansions: Cluster ion polymerization, The Journal of Chemical Physics 138 (12) (2013) 124306.

[7] J. Chan, P. Valencia, L. Zhang, R. Langer, O. Farokhzad, Polymeric nanoparticles for drug delivery, in: S. R. Grobmyer, B. M. Moudgil (Eds.), Cancer Nanotechnology, Vol. 624 of Methods in Molecular Biology, Humana Press, 2010, pp. 163–175.

[8] D. Astruc, Transition-metal nanoparticles in catalysis: From historical background to the state-of-the art, in: Nanoparticles and Catalysis, Wiley-VCH Verlag GmbH Co. KGaA, 2008, pp. 1–48.

[9] U. Banin, O. Millo, S. Dehnen, A. EichhĂ?fer, J. F. Corrigan, O. Fuhr, D. Fenske, K. Blech, M. Homberger, U. Simon, Properties, in: Nanoparticles, Wiley-VCH Verlag GmbH Co. KGaA, 2010, pp. 371–454.

[10] C. Hock, C. Bartels, S. Straßburg, M. Schmidt, H. Haberland, B. von Issendorff, A. Aguado, Premelting and postmelting in clusters, Phys. Rev. Lett. 102 (2009) 043401.

[11] M. Schmidt, R. Kusche, B. von Issendorff, H. Haberland, Irregular variations in the melting point of size-selected atomic clusters, Nature 393 (1998) 238.

[12] C. C. Pradzynski, R. M. Forck, T. Zeuch, P. Slavíček, U. Buck, A fully size-resolved perspective on the crystallization of water clusters, Science 337 (6101) (2012) 1529–1532.

[13] M. R. Hoare, Structure and dynamics of simple microclusters, in: Advances in Chemical Physics, John Wiley Sons, Inc., 2007, pp. 49–135.

[14] H. Pauly, J. Toennies, The study of intermolecular potentials with molecular beams at thermal energies, Vol. 1 of Advances in Atomic and Molecular Physics, Academic Press, 1965, pp. 195 – 344.

[15] L. C. Ch'ng, A. K. Samanta, G. Czakó, J. M. Bowman, H. Reisler, Experimental and theoretical investigations of energy transfer and hydrogen-bond breaking in the water dimer, Journal of the American Chemical Society 134 (37) (2012) 15430–15435.

[16] B. E. Rocher-Casterline, L. C. Ch'ng, A. K. Mollner, H. Reisler, Communication: Determination of the bond dissociation energy (d[sub 0]) of the water dimer, (h[sub 2]o)[sub 2], by velocity map imaging, The Journal of Chemical Physics 134 (21) (2011) 211101.

[17] M. Fárník, Molecular Dynamics in Free Clusters and Nanoparticles Studied in Molecular Beams, ICT Prague Press, Institute of Chemical Technology Prague, 2011.

[18] P. Slavicek, M. Farnik, Photochemistry of hydrogen bonded heterocycles probed by photodissociation experiments and ab initio methods, Phys. Chem. Chem. Phys. 13 (2011) 12123–12137.

[19] E. Becker, K. Bier, W. Henkes, Strahlen aus kondensierten atomen und molekeln im hochvakuum, Zeitschrift fur Physik 146 (1956) 333–338.

[20] E. Becker, On the history of cluster beams, Zeitschrift fur Physik D Atoms, Molecules and Clusters 3 (1986) 101–107.

[21] M. N. R. Ashfold, G. A. King, D. Murdock, M. G. D. Nix, T. A. A. Oliver, A. G. Sage, [small pi][sigma]* excited states in molecular photochemistry, Phys. Chem. Chem. Phys. 12 (2010) 1218–1238.

[22] M. Larsson, A. E. Orel, in: Dissociative Recombination of Molecular Ions, Cambridge University Press, 2008.

[23] M. J. Bastian, R. A. Dressler, D. J. Levandier, E. Murad, F. Muntean, P. B. Armentrout, Low energy collision-induced dissociation and photodissociation studies of the (n[sub 2]o,h[sub 2]o)[sup +] cluster ion, The Journal of Chemical Physics 106 (23) (1997) 9570–9579.

[24] A. I. Krylov, R. B. Gerber, Photodissociation dynamics of hcl in solid ar: Cage exit, nonadiabatic transitions, and recombination, The Journal of Chemical Physics 106 (16) (1997) 6574–6587.

[25] M. Fárník, V. Poterya, O. Votava, M. Ončák, P. Slavíček, I. Dauster, U. Buck, Solvent-induced photostability of acetylene molecules in clusters probed by multiphoton dissociation?, The Journal of Physical Chemistry A 113 (26) (2009) 7322–7330.

[26] M. S. El-Shall, Polymerization in the gas phase, in clusters, and on nanoparticle surfaces, Accounts of Chemical Research 41 (7) (2008) 783–792.

[27] Y. Ono, C. Y. Ng, A study of the unimolecular decomposition of the (c2h2)3+ complex, Journal of the American Chemical Society 104 (18) (1982) 4752–4758.

[28] P. O. Momoh, A. M. Hamid, A.-R. Soliman, S. A. Abrash, M. S. El-Shall, Structure of the c8h8+ radical cation formed by electron impact ionization of acetylene clusters. evidence for a (benzene+ acetylene) complex, The Journal of Physical Chemistry Letters 2 (19) (2011) 2412–2419.

[29] R. A. Relph, J. C. Bopp, J. R. Roscioli, M. A. Johnson, Structural characterization of (c[sub 2]h[sub 2])[sub 1–6][sup +] cluster ions by vibrational predissociation spectroscopy, The Journal of Chemical Physics 131 (11) (2009) 114305.

[30] R. A. Rose, S. J. Greaves, T. A. A. Oliver, I. P. Clark, G. M. Greetham, A. W. Parker, M. Towrie, A. J. Orr-Ewing, Vibrationally quantum-state-specific dynamics of the reactions of cn radicals with organic molecules in solution, The Journal of Chemical Physics 134 (24) (2011) 244503.

[31] D. R. Glowacki, R. A. Rose, S. J. Greaves, A. J. Orr-Ewing, J. N. Harwey, Ultrafast energy flow in the wake of solution-phase bimolecular reactions, Nat Chem 3 (11) (2011) 850.

[32] M. Ončák, P. Slavíček, V. Poterya, M. Fárník, U. Buck, Emergence of charge-transfer-to-solvent band in the absorption spectra of hydrogen halides on ice nanoparticles: Spectroscopic evidence for acidic dissociation, The Journal of Physical Chemistry A 112 (24) (2008) 5344–5353.

[33] M. Ončák, P. Slavíček, M. Fárník, U. Buck, Photochemistry of hydrogen halides on water clusters: Simulations of electronic spectra and photodynamics, and com-

parison with photodissociation experiments, The Journal of Physical Chemistry A 115 (23) (2011) 6155–6168.

[34] B. J. Gertner, J. T. Hynes, Model molecular dynamics simulation of hydrochloric acid ionization at the surface of stratospheric ice, Faraday Discuss. 110 (1998) 301–322.

[35] A. Golan, M. Ahmed, Ionization of water clusters mediated by exciton energy transfer from argon clusters, The Journal of Physical Chemistry Letters 3 (4) (2012) 458–462.

[36] J. Kočišek, J. Fedor, V. Poterya, A. Pysanenko, O. Votava, M. Fárník, UV Photodissociation of Acetylene in Various Environments, MATFYZPRESS Prague, 2011, pp. 241–246.

[37] J. Kočiaek, J. Lengyel, M. Fárník, Benzene Cation from Acetylene Clusters ? Precursor of PAHs in Space, MATFYZPRESS Prague, 2012, pp. 49–53.

[38] J. Kočišek, J. Lengyel, V. Poterya, A. Pysanenko, P. Svrčková, M. Fárník, From gas phase to bulk ? photodissociation of neutral size selected HBrn clusters, MATFYZPRESS Prague, 2013, submitted

[39] J. Kocisek, E. Illenberger, S. Matejcik, Dissociative electron attachment to the silane derivatives trichlorovinylsilane (sicl3c2h3), tetravinylsilane (si(c2h3)(4)) and trimethylvinylsilane (si(ch3)(3)c2h3), Int. J. Mass Spectrom. 315 (2012) 40–45.

[40] J. Kocisek, O. Struzinsky, H. Sahankova, F. Krcma, S. Matejcik, Electron ionization of dimethylphenylsilane - appearance energies of selected ionic fragments, Plasma Process. Polym. 9 (3) (2012) 298–303.

[41] P. Atkins, J. de Paula, Physical Chemistry, W. H. Freeman Co. NY, 2006.

[42] P. L. Houston, Vector correlations in photodissociation dynamics, The Journal of Physical Chemistry 91 (21) (1987) 5388–5397.

[43] J. Turro,V. Ramurthy, J. Scaiano, Photophysical radiationless transitions, in: Principles of Molecular Photochemistry, University Science Books, Sausalito, CA, 2009, pp. 371–454.

[44] T. H. Maiman, Stimulated optical radiation in ruby, Nature 187 (4736) (1960) 493–494.

[45] J. E. Geusic, H. M. Marcos, L. G. V. Uitert, Laser oscillations in nd-doped yttrium aluminum, yttrium gallium and gadolinium garnets, Applied Physics Letters 4 (10) (1964) 182–184.

[46] R. Zare, D. Herschbach, Doppler line shape of atomic fluorescence excited by molecular photodissociation, Proceedings of the IEEE 51 (1) (1963) 173 – 182.

[47] R. N. Zare, P. J. Dagdigian, Tunable laser fluorescence method for product state analysis, Science 185 (4153) (1974) 739 – 747.

[48] J. Solomon, Photodissociation as studied by photolysis mapping, The Journal of Chemical Physics 47 (3) (1967) 889–895.

[49] C. Jonah, P. Chandra, R. Bersohn, Anisotropic photodissociation of cadmium dimethyl, The Journal of Chemical Physics 55 (4) (1971) 1903–1907.

[50] Y. T. Lee, J. D. McDonald, P. R. LeBreton, D. R. Herschbach, Molecular beam reactive scattering apparatus with electron bombardment detector, Review of Scientific Instruments 40 (11) (1969) 1402–1408.

[51] G. E. Busch, R. T. Mahoney, R. I. Morse, K. R. Wilson, Translational spectroscopy: Cl[sub 2] photodissociation, The Journal of Chemical Physics 51 (1) (1969) 449–450.

[52] R. W. Diesen, J. C. Wahr, S. E. Adler, Photochemical recoil spectroscopy, The Journal of Chemical Physics 50 (8) (1969) 3635–3636.

[53] P. Agostini, G. Barjot, G. Mainfray, C. Manus, J. Thebault, Multiphoton ionization of rare gases at 1.06 mum and 0.53 mum, Physics Letters A 31 (7) (1970) 367 – 368.

[54] D. Feldman, R. Lengel, R. Zare, Multiphoton ionization: a method for characterizing molecular beams and beam reaction products, Chemical Physics Letters 52 (3) (1977) 413 – 417.

[55] D. W. Chandler, P. L. Houston, Two-dimensional imaging of state-selected photodissociation products detected by multiphoton ionization, The Journal of Chemical Physics 87 (2) (1987) 1445–1447.

[56] Imaging probes of spectroscopy and dynamics, Phys. Chem. Chem. Phys. 8 (2006) 2905–3036.

[57] B. Whitaker, Imaging in molecular dynamics, Cambridge University Press, 2003, p. 266.

[58] A. Suits, R. Continetti, Imaging in chemical dynamics, American Chemical Society, 2000, p. 411.

[59] A. Eppink, D. Parker, Velocity map imaging of ions and electrons using electrostatic lenses: Application in photoelectron and photofragment ion imaging of molecular oxygen, Review of Scientific Instruments 68 (9) (1997) 3477–3484.

[60] S. Manzhos, H. Loock, Photofragment image analysis using the onion-peeling algorithm, Computer Physics Communications 154 (1) (2003) 76–87.

[61] V. Dribinski, A. Ossadtchi, V. A. Mandelshtam, H. Reisler, Reconstruction of abel-transformable images: The gaussian basis-set expansion abel transform method, Review of Scientific Instruments 73 (7) (2002) 2634–2642.

[62] C. R. Gebhardt, T. P. Rakitzis, P. C. Samartzis, V. Ladopoulos, T. N. Kitsopoulos, Slice imaging: A new approach to ion imaging and velocity mapping, Review of Scientific Instruments 72 (10) (2001) 3848–3853.

[63] D. Townsend, M. P. Minitti, A. G. Suits, Direct current slice imaging, Review of Scientific Instruments 74 (4) (2003) 2530–2539.

[64] J. J. Lin, J. Zhou, W. Shiu, K. Liu, Application of time-sliced ion velocity imaging to crossed molecular beam experiments, Review of Scientific Instruments 74 (4) (2003) 2495–2500.

[65] R. Salman, Vibrationally Mediated Photodissociation, The Royal Society of Chemistry, 2009.

[66] F. F. Crim, Vibrationally mediated photodissociation: Exploring excited-state surfaces and controlling decomposition pathways, Annual Review of Physical Chemistry 44 (1) (1993) 397–428.

[67] H. Reisler, Photofragment spectroscopy and predissociation dynamics of weakly bound molecules, Annual Review of Physical Chemistry 60 (1) (2009) 39–59.

[68] L. C. Ch'ng, A. K. Samanta, Y. Wang, J. M. Bowman, H. Reisler, Experimental and theoretical investigations of the dissociation energy (d0) and dynamics of the water trimer, (h2o)3, The Journal of Physical Chemistry A 0 (0) (2013) null.

[69] B. E. Rocher-Casterline, L. C. Ch'ng, A. K. Mollner, H. Reisler, Communication: Determination of the bond dissociation energy (d[sub 0]) of the water dimer, (h[sub 2]o)[sub 2], by velocity map imaging, The Journal of Chemical Physics 134 (21) (2011) 211101.

[70] L. Poisson, E. Gloaguen, J.-M. Mestdagh, B. Soep, A. Gonzalez, M. Chergui, Direct observation of microscopic solvation at the surface of clusters by ultrafast photoelectron imaging?, The Journal of Physical Chemistry A 112 (39) (2008) 9200–9210.

[71] R. Otto, J. Xie, J. Brox, S. Trippel, M. Stei, T. Best, M. R. Siebert, W. L. Hase, R. Wester, Reaction dynamics of temperature-variable anion water clusters studied with crossed beams and by direct dynamics, Faraday Discuss. 157 (2012) 41–57.

[72] D. Irimia, R. Kortekaas, M. H. M. Janssen, In situ characterization of a cold and short pulsed molecular beam by femtosecond ion imaging, Phys. Chem. Chem. Phys. 11 (2009) 3958–3966.

[73] R. Moshammer, J. Ullrich, M. Unverzagt, W. Schmidt, P. Jardin, R. E. Olson, R. Mann, R. Dörner, V. Mergel, U. Buck, H. Schmidt-Böcking, Low-energy electrons and their dynamical correlation with recoil ions for single ionization of helium by fast, heavy-ion impact, Phys. Rev. Lett. 73 (1994) 3371–3374.

[74] C. S. Lehmann, N. B. Ram, M. H. M. Janssen, Velocity map photoelectron-photoion coincidence imaging on a single detector, Review of Scientific Instruments 83 (9) (2012) 093103.

[75] A. Vredenborg, C. S. Lehmann, D. Irimia, W. G. Roeterdink, M. H. M. Janssen, The reaction microscope: Imaging and pulse shaping control in photodynamics, ChemPhysChem 12 (8) (2011) 1459–1473.

[76] R. N. Zare, ANGULAR MOMENTUM Understanding spatial aspects in chemistry and physics, John Wiley Sons, Inc., 1988.

[77] L. D. A. Siebbeles, M. Glass-Maujean, O. S. Vasyutinskii, J. A. Beswick, O. Roncero, Vector properties in photodissociation: Quantum treatment of the correlation between the spatial anisotropy and the angular momentum polarization of the fragments, The Journal of Chemical Physics 100 (5) (1994) 3610–3623.

[78] J. A. Beswick, R. N. Zare, On the quantum and quasiclassical angular distributions of photofragments, The Journal of Chemical Physics 129 (16) (2008) 164315.

[79] J. Pišút, L. Gomolčák, V. Černý, in: Úvod do kvantovej mechaniky, Alfa, Bratislava, 1983.

[80] R. N. Zare, Photofragment angular distributions from oriented symmetric-top precursor molecules, Chemical Physics Letters 156 (1) (1989) 1 – 6.

[81] T. P. Rakitzis, A. J. van den Brom, M. H. Janssen, Molecular and laboratory frame photofragment angular distributions from oriented and aligned molecules, Chemical Physics Letters 372 (1?2) (2003) 187 – 194.

[82] T. P. Rakitzis, R. N. Zare, Photofragment angular momentum distributions in the molecular frame: Determination and interpretation, The Journal of Chemical Physics 110 (7) (1999) 3341–3350.

[83] A. S. Bracker, E. R. Wouters, A. G. Suits, O. S. Vasyutinskii, Imaging the alignment angular distribution: State symmetries, coherence effects, and nonadiabat-

ic interactions in photodissociation, The Journal of Chemical Physics 110 (14) (1999) 6749–6765.

[84] T. Rakitzis, P. Samartzis, R. Toomes, L. Tsigaridas, M. Coriou, D. Chestakov, A. Eppink, D. Parker, T. Kitsopoulos, Photofragment alignment from the photodissociation of {HCl} and {HBr}, Chemical Physics Letters 364 (1?2) (2002) 115 – 120.

[85] A. Brown, Photodissociation of hi and di: Polarization of atomic photofragments, The Journal of Chemical Physics 122 (8) (2005) 084301.

[86] P. M. Regan, S. R. Langford, A. J. Orr-Ewing, M. N. R. Ashfold, The ultraviolet photodissociation dynamics of hydrogen bromide, J. Chem. Phys. 110 (1) (1999) 281–288.

[87] E. Roberts, S. Cavanagh, S. Gibson, B. Lewis, C. Dedman, G. Picker, Achieving high signal-to-noise performance for a velocity-map imaging experiment, Journal of Electron Spectroscopy and Related Phenomena 144?147 (0) (2005) 251 – 254, proceeding of the Fourteenth International Conference on Vacuum Ultraviolet Radiation Physics.

[88] H. T. Liou, S. F. Chiou, K. L. Huang, Ozone yields from oxygen irradiated at 193 nm, Ozone: Science Engineering 19 (3) (1997) 273–280.

[89] B.-Y. Chang, R. C. Hoetzlein, J. A. Mueller, J. D. Geiser, P. L. Houston, Improved two-dimensional product imaging: The real-time ion-counting method, Review of Scientific Instruments 69 (4) (1998) 1665–1670.

[90] C. Brion, M. Dyck, G. Cooper, Absolute photoabsorption cross-sections (oscillator strengths) for valence and inner shell excitations in hydrogen chloride, hydrogen bromide and hydrogen iodide, Journal of Electron Spectroscopy and Related Phenomena 144?147 (0) (2005) 127 – 130, proceeding of the Fourteenth International Conference on Vacuum Ultraviolet Radiation Physics.

[91] VPL Molecular Spectroscopic Database.
URL `http://vpl.astro.washington.edu/spectra/hbr.htm`

[92] P. Linstrom, W. Mallard, in: NIST Chemistry WebBook, NIST Standard Reference Database Number 69, National Institute of Standards and Technology, Gaithersburg MD, 20899, 2013.
URL `http://webbook.nist.gov`

[93] Occupational health guideline for hydrogen bromide, The National Institute for Occupational Safety and Health publication no 81-123.
URL `http://www.cdc.gov/niosh/docs/81-123/pdfs/0331.pdf`

[94] R. S. Mulliken, Low electronic states of simple heteropolar diatomic molecules: Iii. hydrogen and univalent metal halides, Phys. Rev. 51 (1937) 310–332.

[95] J. M. Brown, A. Carrington, Coupling of electronic and rotational motion: Hund's coupling cases, in: Rotational Spectroscopy of Diatomic Molecules, Cambridge University Press, 2010, pp. 224–232.

[96] J. Zhang, C. W. Riehn, M. Dulligan, C. Wittig, An experimental study of hf photodissociation: Spin–orbit branching ratio and infrared alignment, The Journal of Chemical Physics 104 (18) (1996) 7027–7035.

[97] E. Nikitin, R. Zare, Correlation diagrams for hund's coupling cases in diatomic molecules with high rotational angular momentum, Molecular Physics 82 (1) (1994) 85–100.

[98] A. G. Smolin, O. S. Vasyutinskii, G. G. Balint-Kurti, A. Brown, Photodissociation of hbr. 1. electronic structure, photodissociation dynamics, and vector correlation coefficients?, The Journal of Physical Chemistry A 110 (16) (2006) 5371–5378.

[99] R. Baumfalk, U. Buck, C. Frischkorn, S. Gandhi, C. Lauenstein, {UV} photolysis of (hbr)n clusters with known size distribution, Chemical Physics Letters 269 (3?4) (1997) 321 – 326.

[100] R. Baumfalk, U. Buck, Photodissociation of hbr molecules and clusters: Anisotropy parameters, branching ratios, and.., Journal of Chemical Physics 111 (6) (1999) 2595.

[101] R. Baumfalk, N. Hendrik Nahler, U. Buck, Vibrational excitation and caging following the photodissociation of small hbr clusters in and on large ar clusters, Phys. Chem. Chem. Phys. 3 (2001) 2372–2377.

[102] R. Baumfalk, N. Hendrik Nahler, U. Buck, Photodissociation and caging of hbr and hi molecules on the surface of large rare gas clusters, Faraday Discuss. 118 (2001) 247–256.

[103] U. Buck, Photodissociation of hydrogen halide molecules in different cluster environments, The Journal of Physical Chemistry A 106 (43) (2002) 10049–10062.

[104] N. Hendrik Nahler, R. Baumfalk, U. Buck, H. Vach, P. Slavicek, P. Jungwirth, Photodissociation of hbr in and on ar clusters: the role of the position of the molecule, Phys. Chem. Chem. Phys. 5 (2003) 3394–3401.

[105] M. Fárník, N. H. Nahler, U. Buck, P. Slavíček, P. Jungwirth, Photodissociation of {HBr} on the surface of arn clusters at 193xa0;nm, Chemical Physics 315 (1?2) (2005) 161 – 170.

[106] P. Slavíček, P. Jungwirth, M. Lewerenz, N. H. Nahler, M. Fárník, U. Buck, Pickup and photodissociation of hydrogen halides in floppy neon clusters, The Journal of Physical Chemistry A 107 (39) (2003) 7743–7754.

[107] V. Poterya, M. Farnik, P. SlaviCek, U. Buck, V. V. Kresin, Photodissociation of hydrogen halide molecules on free ice nanoparticles, The Journal of Chemical Physics 126 (7) (2007) 071101.

[108] M. Ryazanov, H. Reisler, Improved sliced velocity map imaging apparatus optimized for h photofragments, The Journal of Chemical Physics 138 (14) (2013) 144201.

[109] D. J. Auerbach, Velocity measurements by time-of-flight methods, in: G. Scoles (Ed.), Atomic and Molecular Beam Methods, Vol. I, Oxford, New York, 1988, p. 362.

[110] U. Buck, H. Meyer, Scattering analysis of cluster beams: formation and fragmentation of small ar_n clusters, Phys. Rev. Lett. 52 (1984) 109.

[111] P. Piseri, H. V. Tafreshi, P. Milani, Manipulation of nanoparticles in supersonic beams for the production of nanostructured materials, Current Opinion in Solid State and Materials Science 8 (3?4) (2004) 195 – 202.

[112] W. Schöllkopf, J. P. Toennies, Nondestructive mass selection of small van der waals clusters, Science 266 (5189) (1994) 1345–1348.

[113] B. S. Zhao, S. A. Schulz, S. A. Meek, G. Meijer, W. Schöllkopf, Quantum reflection of helium atom beams from a microstructured grating, Phys. Rev. A 78 (2008) 010902.

[114] B. S. Zhao, G. Meijer, W. Schöllkopf, Quantum reflection of he2 several nanometers above a grating surface, Science 331 (6019) (2011) 892–894.

[115] S. Gerlich, M. Gring, H. Ulbricht, K. Hornberger, J. Tüxen, M. Mayor, M. Arndt, Matter-wave metrology as a complementary tool for mass spectrometry, Angewandte Chemie International Edition 47 (33) (2008) 6195–6198.

[116] P. Haslinger, N. Dorre, P. Geyer, J. Rodewald, S. Nimmrichter, M. Arndt, A universal matter-wave interferometer with optical ionization gratings in the time domain, Nat Phys 9 (3) (2013) 1745–2473.

[117] J. Fedor, V. Poterya, A. Pysanenko, M. Farnik, Cluster cross sections from pickup measurements: Are the established methods consistent?, The Journal of Chemical Physics 135 (10) (2011) 104305.

[118] E. Loginov, L. F. Gomez, A. F. Vilesov, Surface deposition and imaging of large ag clusters formed in he droplets, The Journal of Physical Chemistry A 115 (25) (2011) 7199–7204.

[119] L. Ambrosone, A. Ceglie, G. Colafemmina, G. Palazzo, General methods for determining the droplet size distribution in emulsion systems, The Journal of Chemical Physics 110 (2) (1999) 797–804.

[120] W. Li, S. D. Chambreau, S. A. Lahankar, A. G. Suits, Megapixel ion imaging with standard video, Review of Scientific Instruments 76 (6) (2005) 063106.

[121] P. Mazarov, Charakterisierung eines Flugzeitmassenspektrometers und seine Anwendungen in der Festkörperoberflächenuntersuchung, Duisburg, Essen, Univ., Diss, Universität Duisburg-Essen, 2006.

[122] J. A. Booze, T. Baer, On the determination of cluster properties by ionization techniques, The Journal of Chemical Physics 96 (7) (1992) 5541–5543.

[123] A. Shard, I. Gilmore, Analysis of metastable ions in the tof-sims spectra of polymers, International Journal of Mass Spectrometry 269 (1?2) (2008) 85 – 94.

[124] H. Schöbel, P. Bartl, C. Leidlmair, S. Denifl, O. Echt, T. Märk, P. Scheier, High-resolution mass spectrometric study of pure helium droplets, and droplets doped with krypton, The European Physical Journal D 63 (2) (2011) 209–214.

[125] O. Echt, P. D. Dao, S. Morgan, J. A. W. Castleman, Multiphoton ionization of ammonia clusters and the dissociation dynamics of protonated cluster ions, The Journal of Chemical Physics 82 (9) (1985) 4076–4085.

[126] S. Wei, W. B. Tzeng, J. A. W. Castleman, Dissociation dynamics: Measurements of decay fractions of metastable ammonia cluster ions, The Journal of Chemical Physics 93 (4) (1990) 2506–2512.

[127] D. H. Mordaunt, M. N. R. Ashfold, Near ultraviolet photolysis of c[sub 2]h[sub 2]: A precise determination of d[sub 0](hcc - h), The Journal of Chemical Physics 101 (3) (1994) 2630–2631.

[128] Acetylene material safety data sheet (1995) 4.
URL `www.stoodyind.com/safety/msds/Acetylene.pdf?`

List of Tables

List of Figures

List of Abbreviations

AIM = Apparatus for IMaging
AC = Alternating Current
BNC = Bayonet Neill?Concelman (connector type)
BASEX = BAsis Set EXpansions (image transformation)
CCD = Charge Coupled Device
CluB = Cluster Beam (apparatus)
DC = Direct Current
DMSO = DiMethyl SulfOxide (solvent)
HV = High Voltage
IESL = The Institute of Electronic Structure and Lasers (Crete,GR)
IR = Infra Red
KED = Kinetic Energy Distribution
KF = Klein Flange (vacuum connection)
LASER = Light Amplification by Stimulated Emission of Radiation
MCP = Micro Channel Plate
OPO = Optical Parametric Oscillator
QM = Quantum Mechanics
Rg = Rare Gas
REMPI = Resonance Enhanced Multiphoton Ionization
SHV = Safe High Voltage (connector type)
TKER = Total Kinetic Energy Released
TOF = Time Of Flight
UV = Ultra Violet
VMI = Velocity Map Imaging
VMP = Vibrationally Mediated Photodissociation

Attachments

1. Velocity map imaging of HBr photodissociation in large rare gas clusters

2. Caging of Cl atom from photodissociation of CF2Cl2 in clusters

3. Short review on the acetylene photochemistry in clusters: photofragment caging and reactivity

4. UV Photodissociation of Acetylene in Various Environments

5. Ionization of large homogeneous and heterogeneous clusters generated in acetylene–Ar expansions: Cluster ion polymerization